

1 **Low levels of nitryl chloride at ground level: Nocturnal**
2 **nitrogen oxides in the Lower Fraser Valley of British**
3 **Columbia**

4 **Hans D. Osthoff¹, Charles A. Odame-Ankrah¹, Youssef M. Taha¹,**
5 **Travis W. Tokarek¹, Corinne L. Schiller², Donna Haga³, Keith Jones², and**
6 **Roxanne Vingarzan²**

7 [1] {Department of Chemistry, University of Calgary, Calgary, Alberta T2N 1N4,
8 Canada}

9 [2] {Applied Science Division, Prediction and Services West, Meteorological Service
10 of Canada, Environment and Climate Change Canada, Vancouver, British Columbia
11 V6C 3S5, Canada}

12 [3] {British Columbia Ministry of Environment and Climate Change Strategy,
13 Cranbrook, British Columbia V1C 7G5, Canada}

14 Correspondence to: H. D. Osthoff (hosthoff@ucalgary.ca)

15 **Abstract**

16
17 The nocturnal nitrogen oxides, which include the nitrate radical (NO_3), dinitrogen pentoxide
18 (N_2O_5), and its uptake product on chloride containing aerosol, nitryl chloride (ClNO_2), can
19 have profound impacts on the lifetime of NO_x ($= \text{NO} + \text{NO}_2$), radical budgets, and next-day
20 photochemical ozone (O_3) production, yet their abundances and chemistry are only sparsely
21 constrained by ambient air measurements.

22 Here, we present a measurement data set collected at a routine monitoring site near the
23 Abbotsford International Airport (YXX) located approximately 30 km from the Pacific Ocean
24 in the Lower Fraser Valley (LFV) on the West coast of British Columbia. Measurements were
25 made from July 20 to August 4, 2012, and included mixing ratios of ClNO_2 , N_2O_5 , NO , NO_2 ,
26 total odd nitrogen (NO_y), O_3 , photolysis frequencies, and size distribution and composition of
27 non-refractory submicron aerosol (PM_{10}).

28 At night, O₃ was rapidly and often completely removed by dry deposition and by titration
29 with NO of anthropogenic origin and unsaturated biogenic hydrocarbons in a shallow
30 nocturnal inversion surface layer. The low nocturnal O₃ mixing ratios and presence of strong
31 chemical sinks for NO₃ limited the extent of nocturnal nitrogen oxide chemistry at ground
32 level. Consequently, mixing ratios of N₂O₅ and ClNO₂ were low (<30 and <100 parts-per-
33 trillion by volume (pptv) and median nocturnal peak values of 7.8 pptv and 7.9 pptv,
34 respectively). Mixing ratios of ClNO₂ frequently peaked 1 - 2 hours after sunrise rationalized
35 by more efficient formation of ClNO₂ in the nocturnal residual layer aloft than at the surface
36 and the breakup of the nocturnal boundary layer structure in the morning. When quantifiable,
37 production of ClNO₂ from N₂O₅ was efficient and likely occurred predominantly on
38 unquantified supermicron sized or refractory sea salt derived aerosol. After sunrise,
39 production of Cl radicals from photolysis of ClNO₂ was negligible compared to production of
40 OH from the reaction of O(¹D) + H₂O except for a short period after sunrise.

41

42 **Keywords**

43 Lower Fraser Valley, ClNO₂, surface measurements, nocturnal residual layer, ClNO₂ morning
44 peak, vertical entrainment

45

46 1 Introduction

47 The Lower Fraser Valley (LFV) is prone to episodes of poor air quality, in part because of its
48 geography which facilitates stagnation periods and accumulation of airborne pollutants
49 through processes such as the Wake-Induced Stagnation Effect (Brook et al., 2004), and also
50 because of continued growth of human population and associated emissions from urban,
51 suburban, agricultural and marine sources. Of special concern have been repeated
52 exceedances of the Canada-Wide Standard and, as of 2012, the Canadian Ambient Air
53 Quality Standards (CAAQS) for fine particulate matter (PM_{2.5}) and ozone (O₃) at Chilliwack
54 and Hope, located in the eastern part of the LFV downwind of Vancouver (Ainslie et al.,
55 2013). These exceedances have occurred in spite of ongoing declines in emissions of both
56 nitrogen oxides (NO_x = NO + NO₂) and volatile organic compounds (VOCs) resulting from
57 the introduction of new vehicle standards and (now discontinued) local vehicle emission
58 testing programs (Ainslie et al., 2013). Previous large-scale studies in the LFV such as Pacific
59 1993 (Steyn et al., 1997), the Regional Visibility Experimental Assessment in the Lower
60 Fraser Valley (REVEAL) I and II (Pryor et al., 1997; Pryor and Barthelmie, 2000) and Pacific
61 2001 (Vingarzan and Li, 2006) have added important information regarding atmospheric
62 processes leading to O₃ and aerosol formation and visibility issues. However, the
63 transformation of primary (e.g., NO_x, VOCs, SO₂, NH₃, etc.) to secondary pollutants (i.e., O₃
64 and fine particulate matter) is highly complex, and the scientific understanding of these highly
65 non-linear processes remains incomplete.

66 A complicating factor in the LFV is the interaction of anthropogenic emissions with marine
67 derived sea salt aerosol. While sea spray aerosol is a primary source of particulate matter
68 (PM) and hence directly affect particle concentrations and mass loadings (Pryor et al., 2008)
69 and aerosol chloride concentrations (Anlauf et al., 2006) in the LFV, there is now
70 considerable evidence from modeling (Knipping and Dabdub, 2003), laboratory (Raff et al.,
71 2009), and field studies (Tanaka et al., 2003; Osthoff et al., 2008) that "active chlorine"
72 species released from sea salt can negatively affect air quality and promote O₃ and secondary
73 aerosol formation in coastal regions.

74 In an analysis of 20 years of O₃ air quality data in the LFV region, Ainslie and Steyn (2007)
75 concluded that precursor buildup, prior to an exceedance day, plays an important role in the
76 spatial O₃ pattern on exceedance days. Secondary processes involving active chlorine

77 produced from the interaction of marine aerosol with anthropogenic pollution would fit this
78 profile but are not currently constrained by measurements.

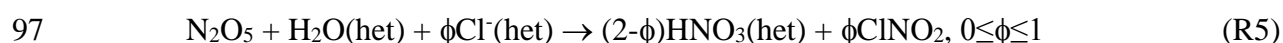
79 One pathway to activate chlorine from sea salt is the reactive uptake of dinitrogen pentoxide
80 (N_2O_5) on chloride containing aerosol to yield nitryl chloride (ClNO_2) (Behnke et al., 1997;
81 Finlayson-Pitts et al., 1989). Briefly, N_2O_5 is formed from the reversible reaction of nitrogen
82 dioxide (NO_2) with the photo-labile nitrate radical (NO_3 ; R1), which in turn is formed from
83 reaction of NO_2 with O_3 (R2).



86 In ambient air, N_2O_5 , NO_3 and NO_2 are usually in equilibrium; the equilibrium constant, K_2 , is
87 temperature dependent, favoring NO_3 and NO_2 at higher temperatures (Osthoff et al., 2007).
88 During daytime, NO_3 (and, indirectly, N_2O_5) is removed primarily via its reaction (R3) with
89 NO (which is generated from NO_2 photolysis and directly emitted, for example, by
90 automobiles) and by NO_3 photolysis (R4) (Wayne et al., 1991).



93 The heterogeneous hydrolysis of N_2O_5 to nitric acid (HNO_3) is an important nocturnal NO_x
94 and odd oxygen ($\text{O}_x = \text{NO}_2 + \text{O}_3$) removal pathway (Chang et al., 2011; Brown et al., 2006a).
95 On chloride containing aerosol, however, uptake of N_2O_5 yields up to a stoichiometric amount
96 of ClNO_2 (R5) (Behnke et al., 1997; Finlayson-Pitts et al., 1989):



98 The ClNO_2 yield, ϕ , is primarily a function of aerosol chloride and water content (Behnke et
99 al., 1997; Bertram and Thornton, 2009; Roberts et al., 2009; Ryder et al., 2014; Ryder et al.,
100 2015b; Ryder et al., 2015a). Formation of ClNO_2 impacts air quality in the following ways:
101 Since ClNO_2 is long-lived at night, its primary fate is photo-dissociation (to Cl and NO_2) in
102 the morning hours after sunrise (R6) (Osthoff et al., 2008).



104 This reaction increases the morning abundance of O_x , leading to greater net photochemical O_3
105 production throughout the day. The other photo fragment, the Cl atom, is highly reactive

106 towards hydrocarbons and will initiate radical chain reactions that produce O₃ and secondary
107 aerosol (Behnke et al., 1997; Young et al., 2014). The fate and impact of ClNO₂ is thus
108 similar to that of nitrous acid (HONO), which also accumulates during the night and
109 photodissociates in the morning to release NO and the hydroxyl radical (OH) that go on to
110 produce O₃ (Alicke et al., 2003).

111 Data collected during the 2006 Texas Air Quality Study – Gulf of Mexico Atmospheric
112 Composition and Climate Study (TEXAQS-GOMACCS) have shown that ClNO₂ production
113 is efficient in the nocturnal polluted marine boundary layer even on primarily non-sea salt
114 aerosol surfaces (Osthoff et al., 2008). As a result, up to 15% of total odd nitrogen (NO_y) was
115 present in the form ClNO₂ at night (Osthoff et al., 2008). The high efficiency of ClNO₂
116 formation on aerosol of medium-to-low total chloride content has been confirmed by several
117 laboratory investigations (Bertram and Thornton, 2009; Raff et al., 2009; Roberts et al., 2009)
118 and direct measurements of N₂O₅ uptake on ambient particles (Riedel et al., 2012b). Some
119 ambiguity remains as to the detailed mechanism of R5, but there is agreement that acid
120 displacement of HCl from supermicron (predominantly sea salt aerosol) to submicron
121 (predominantly non-sea salt aerosol) is a key step in the efficient production of ClNO₂. These
122 results suggested that this chemistry is active anywhere where pollution in the form of NO_x
123 and O₃ comes in contact with marine air, including the LFV.

124 However, while the yield of ClNO₂ in reaction R5 is high in polluted coastal regions, the
125 ClNO₂ yield relative to the amount of NO₃ produced via R1 cannot be easily predicted
126 because NO₃ is consumed by reactions with VOCs (R7), e.g., with biogenic VOCs such as
127 isoprene and monoterpenes as well as aldehydes, and dimethyl sulfide (Wayne et al., 1991).



129 Previous studies in the LFV have shown high biogenic VOC concentrations (Biesenthal et al.,
130 1997; Gurren et al., 1998; Drewitt et al., 1998) yet there was active nighttime nitrogen oxide
131 chemistry and aerosol chloride present mainly as sea salt derived aerosol in >1 μm diameter
132 aerosol (Anlauf et al., 2006). During the Pacific 2001 study, measurements of the mixing
133 ratios of NO, NO₂, peroxyacetic nitric anhydride (CH₃C(O)O₂NO₂, PAN), HONO, HNO₃,
134 and NO_y at three ground sites in the LFV indicated deficits of up to 15% in the nocturnal NO_y
135 budget (Hayden et al., 2004) attributable to unquantified species such as alkyl nitrates, N₂O₅,
136 and ClNO₂. McLaren and coworkers quantified mixing ratios of NO₂ and NO₃ by differential
137 optical absorption spectroscopy (DOAS) at the Sumas Eagle Ridge site (~250 m above the

138 floor of the LFV) as part of Pacific 2001 (McLaren et al., 2004) and off-shore on Saturna
139 Island (Figure 1) in the Strait of Georgia in 2005 (McLaren et al., 2010). The LFV data
140 showed occasional episodes of active nocturnal nitrogen oxide chemistry in the residual layer
141 with N₂O₅ contributing up to 9% of NO_y, while the Saturna Island data showed NO₃ mixing
142 ratios of > 20 parts-per-trillion by volume (10⁻¹², pptv) every night of measurement. McLaren
143 et al. estimated that between 0.3 and 1.9 ppbv of ClNO₂ would be produced under these
144 conditions (2010). Efficient formation of ClNO₂ would be consistent with the unidentified O₃
145 precursor proposed by Ainslie and Steyn and is also a plausible explanation for part of the
146 deficit in the NO_y budget observed by Hayden et al. (2004).

147 Another feature of the LFV are somewhat unusual diurnal profiles arising from the vertical
148 structure in pollutant concentrations. Measurements of O₃ and NO₂ using tethered balloons by
149 Pisano et al. (1997) during Pacific 93 at the Harris Road site (located ~38 km NW of
150 Abbotsford International Airport) revealed a highly stratified boundary layer with a shallow,
151 50 m deep isothermal surface layer (also called a nocturnal boundary layer, or NBL) and low
152 surface O₃ concentrations at night. Nocturnal loss of surface O₃ is known to occur by several
153 pathways, including dry deposition, titration with NO (R8), and reaction with unsaturated
154 biogenic hydrocarbons (Neu et al., 1994; Kleinman et al., 1994; Trainer et al., 1987; Logan,
155 1989; Talbot et al., 2005). Titration of O₃ with NO is readily quantified as the concentration
156 of a product of R8, NO₂, can be measured directly and conserves O_x.



158 Usually, the major nocturnal sink of O_x is dry deposition of O₃ and NO₂ (Lin et al., 2010).

159 The balloon data also showed pools of NO₂ and O₃ in a ~100 m deep nocturnal residual layer
160 (NRL) located 200 to 350 m above ground. Following the break-up of the nocturnal layers in
161 the early morning, vertical down-mixing events of O₃ pollution were observed (McKendry et
162 al., 1997). In this process, pollutants are entrained into the growing mixed layer from the
163 NRL, i.e., the growing mixed layer in the hours after sunrise erodes the somewhat deeper
164 NRL, and pollutants are mixed to the surface (Neu et al., 1994; Kleinman et al., 1994).

165 In this manuscript, we present the first measurements of ClNO₂ and N₂O₅ mixing ratios in the
166 LFV. The data were collected at a surface site east of the Abbotsford International Airport
167 (International Air Transport Association (IATA) airport code YXX) located approximately
168 35 km from the Pacific Ocean from July 20 to August 5, 2012. Auxiliary measurements

169 included NO, NO₂, NO_y, O₃, photolysis frequencies, and non-refractory PM₁ aerosol
170 composition and size distributions. An analysis of nocturnal nitrogen oxide chemistry
171 including the formation of ClNO₂ and its potential impact on nocturnal O₃ and NO₂ loss and
172 radical budgets in the LFV are presented.

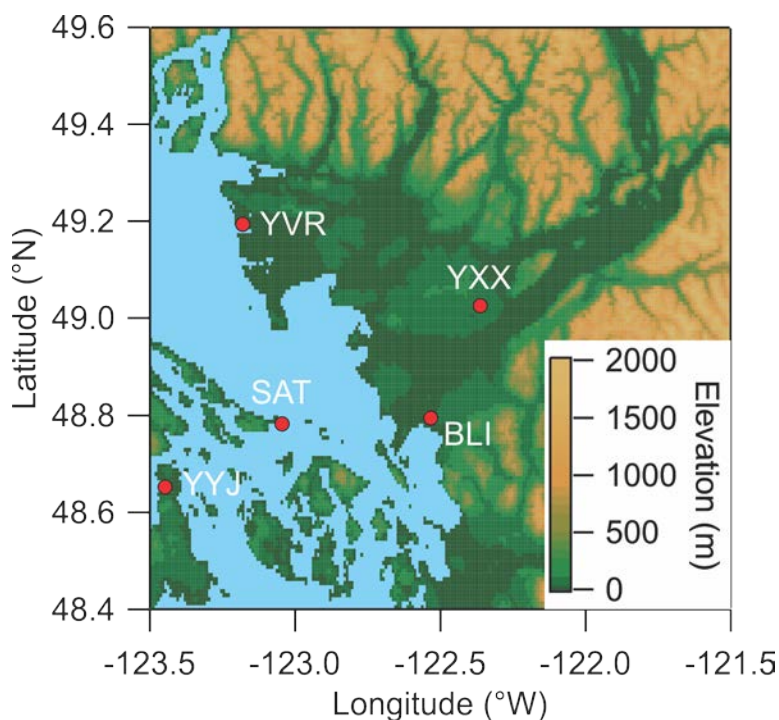
173

174 **2 Experimental**

175 **2.1 Location**

176 The map shown in Figure 1 indicates the location of the study. Ambient air measurements
177 were conducted at the T45 routine monitoring site located to the east YXX at latitude 49.0212
178 (N) and longitude -122.3267 (W) and ~60 m above sea level (ASL) and ~30 km from the
179 Pacific Ocean. A raspberry field was located immediately to the W between the end of the
180 airport runway and the measurement site. Nearby local sources included agricultural
181 operations (such as poultry farms) and emissions from motor vehicle traffic on secondary
182 roads and highways. YXX is located ~60 km ESE of the Vancouver International Airport
183 (YVR) and the City of Vancouver. Abbotsford is in the heart of the so-called "Lower
184 Mainland", the low-lying region stretching from Pacific Ocean at Vancouver to the NW and
185 the Canada-USA border to the S (north of Bellingham, BLI) to the eastern end of the Fraser
186 Valley with a total population in excess of 2,500,000.

187



188

189 **Figure 1.** Map of the Lower Fraser Valley. YXX = Abbotsford International Airport
190 (measurement location for this study). YVR = Vancouver Int'l Airport. YYJ = Victoria Int'l
191 Airport. BLI = Bellingham Int'l Airport. SAT = Saturna Island.

192

193 **2.2 Measurement techniques**

194 The measurement techniques used for this study are listed in Table 1. Data were averaged to 5
195 min prior to presentation.

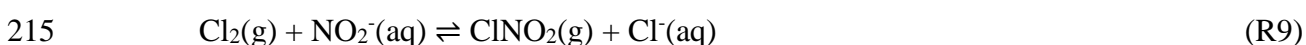
196 The instruments measuring O₃ and nitrogen oxides were housed in an air-conditioned trailer
197 and sampled from a common 0.635 cm (¼") outer diameter (o.d.) and 0.476 cm (3/16") inner
198 diameter (i.d.) Teflon™ inlet at a height of 4 m above ground; the setup is depicted in Figure
199 3 of Tokarek et al. (2014). A scroll pump whose flow rate was throttled using a 50 standard
200 liters per minute (slpm) capacity mass flow controller was connected to the end of the
201 common inlet to minimize the residence time of the sampled air and to reduce inlet "aging",
202 i.e., accumulation of aerosol on filters of individual instruments, whose inlets tapped into the
203 main inlet line at 90°. The total inlet flow was in the range of 18 to 20 slpm.

204 Measurements of PM₁ aerosol composition and size distributions (section 2.3) and of
205 meteorological data were made from the research trailer housing the routine measurements at
206 the site. The Agilent VOC measurements were made from a research trailer owned by
207 Environment and Climate Change Canada (ECCC).

208

209 **2.2.1 Quantification of ClNO₂ by iodide chemical ionization mass spectrometry**

210 Mixing ratios of ClNO₂ were quantified as iodide cluster ions at *m/z* 208 using the "THS
211 Instruments" iodide chemical ionization mass spectrometer (iCIMS) described by Mielke et
212 al. (2011) and calibrated using the scheme by Thaler et al. (2011). In this method, a gas
213 stream containing ClNO₂ is generated from reaction of Cl₂ (Praxair, 10 ppmv in N₂) with an
214 aqueous slurry saturated with NaNO₂ (Sigma-Aldrich) (R9):



216 This gas stream was periodically added to the main inlet with the aid of a normally-open 2-
217 way valve connected to a vacuum pump in a similar fashion as described earlier for N₂O₅ and
218 PAN (Tokarek et al., 2014; Odame-Ankrah and Osthoff, 2011). The ClNO₂ content of the
219 calibration gas stream was quantified by thermal dissociation cavity ring-down spectroscopy
220 (TD-CRDS) as described in section 2.2.2. In total, 31 calibrations for ClNO₂ were carried out,
221 spread out evenly over the measurement period. The iCIMS response factor at *m/z* 208 was
222 (0.40±0.06) Hz pptv⁻¹ (where the error represents the standard deviation of repeated
223 calibrations), normalized to 10⁶ counts of reagent ion at *m/z* 127. The ³⁷ClNO₂I⁻ ion at *m/z* 210

224 was also monitored and found to be (0.298 ± 0.004) times the signal at m/z 208 ($r^2 = 0.944$),
225 slightly lower than Standard Mean Ocean Chloride ^{37}Cl mole fraction in sea water of ~ 0.319
226 (Wieser and Berglund, 2009) and our previously observed ratios of 0.315 ± 0.003 in Calgary
227 (Mielke et al., 2011) and 0.3065 ± 0.0002 in Pasadena (Mielke et al., 2013). The reason(s) for
228 these differences are unclear but may be a result of fractionation processes (Koehler and
229 Wassenaar, 2010; Volpe et al., 1998), a topic outside the scope of this manuscript.

230 The iCIMS was also used to quantify mixing ratios of PAN at m/z 59 and PPN at m/z 73
231 (Slusher et al., 2004; Mielke et al., 2011; Mielke and Osthoff, 2012). For this reason, part of
232 the instrument's inlet prior to the ion-molecule reaction region was heated to $190\text{ }^\circ\text{C}$ to
233 dissociate PANs into their respective carboxylates. Further, the collisional dissociation
234 chamber (CDC) was operated in declustering mode (-22.7 V) to break up ion clusters.
235 Calibrations and matrix effect correction procedures and a time series of the PAN and PPN
236 data were presented by Tokarek et al. (2014).

237

238 2.2.2 Quantification of NO_2 and N_2O_5 by cavity ring-down spectroscopy

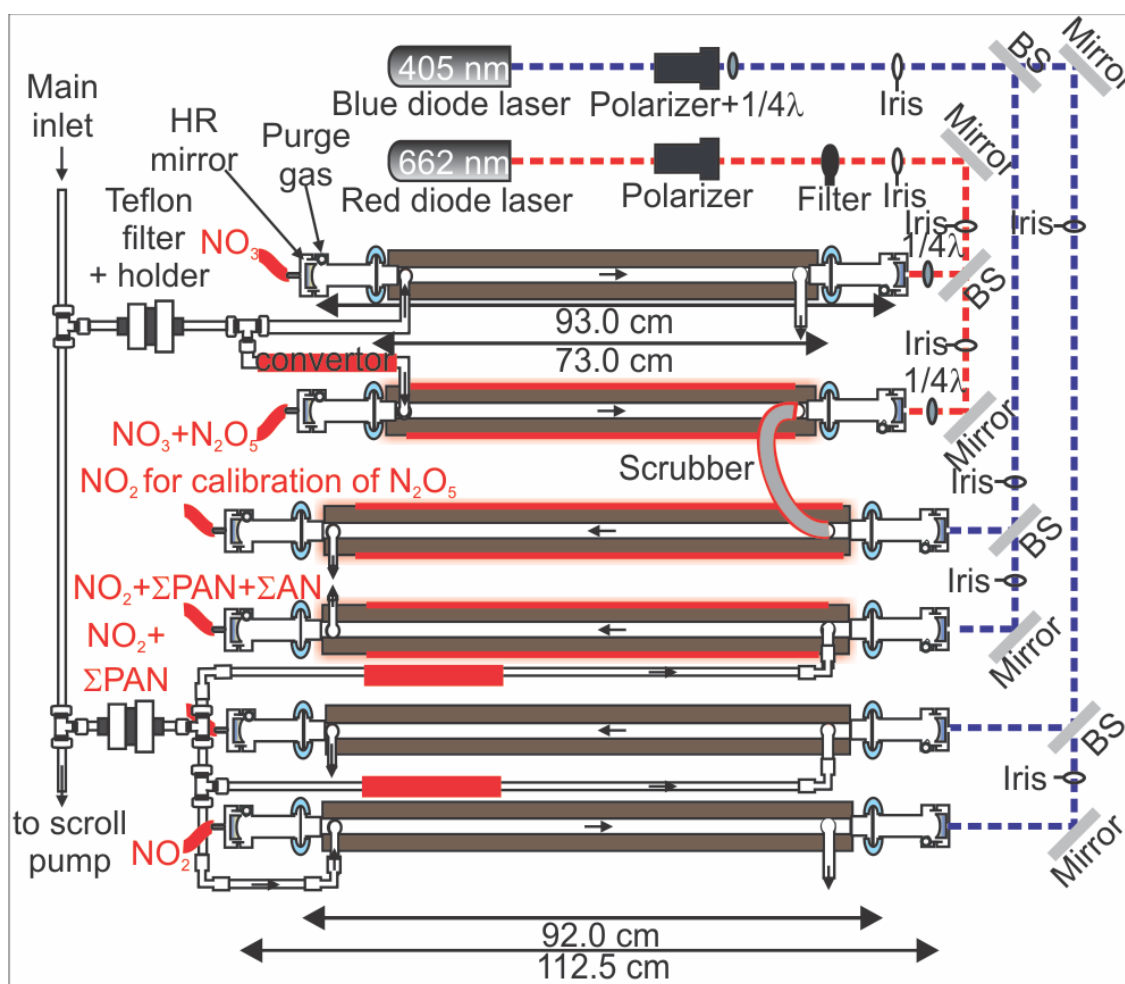
239 The CRDS used in this work was an amalgamated version of two instruments described
240 earlier (Paul and Osthoff, 2010; Odame-Ankrah and Osthoff, 2011), called "Improved
241 Detection Instrument for Nitrogen Oxide Species" (iDinos) (Odame-Ankrah, 2015). A
242 schematic of the optical layout is shown in Figure 2. The optical bread board, instrument
243 frame, electronic and data acquisition components were as described by Paul and Osthoff
244 (2010). The new instrument was set up with up to six parallel detection channels: four 405 nm
245 "blue" diode laser CRDS cells for quantification at NO_2 via its absorption at 405 nm with a
246 distance between the pairs of high-reflectivity (HR) mirrors (Advanced Thin Films) of 112.5
247 cm, of which 92.0 cm were filled with sample air, and two newly constructed 662 nm "red"
248 diode laser CRDS cells for quantification at NO_3 via its absorption at 662 nm with a distance
249 between the HR mirrors (Los Gatos) of 93.0 cm of which 73.0 cm were filled with sample air.
250 Light exiting the far ends of the CRDS cells was collected using fixed-focus collimating
251 lenses and multimode optical fibers (Thorlabs) connected to photomultiplier tubes (PMT,
252 Hamamatsu H9433-03MOD) with 10 MHz bandwidth. Bandpass filters (Thorlabs FB405-10
253 and FB660-10) were placed between the PMTs and the end of the optical fibers.

254 The two laser diodes were simultaneously square-wave modulated by a function generator
255 (SRS DS335). The PMT voltages were digitized using an 8-channel 14-bit data acquisition

256 card (National Instruments PCI-6133; 2.5 MS s^{-1} simultaneous sampling sample rate)
257 connected to a laptop computer via a PCMCIA-to-PCI expansion unit (Magma CB4DRQ) and
258 controlled by software written in LABVIEW™ (National Instruments).

259 Ring-down time constants (τ) were determined from a linear fit to the logarithm of the
260 digitized PMT voltage as described by *Brown et al.* (2002) immediately after acquisition of
261 the ring-down traces (which were co-added to a user-selectable averaging time prior to the
262 fit). The fitting algorithm requires the subtraction of the PMT voltage offset prior to taking the
263 logarithm; this offset was measured between ring-down events after the signal had returned to
264 baseline, which limited the repetition rate of the diode lasers and the number of traces
265 averaged per second to a frequency of 300 Hz.

266



267
268 **Figure 2.** Optical layout of the cavity ring-down spectrometer. $1/4\lambda$ = quarter wave plate. BS =
269 beam splitter. HR mirror = high reflectivity mirror. Drawing is not to scale.

270

271 Ring-down time constants in the absence of the target absorber (τ_0) were determined by
272 flooding the inlet (each once per hour) with ultra-pure, or "zero", air (Praxair) for the 405 nm
273 channels and by titration with NO for the 662 nm channel (Brown et al., 2001; Simpson,
274 2003) Typical values of τ_0 were in the range of 63 to 67 μ s and between 198 and 210 μ s for
275 the blue and red channels, respectively. The baseline precision (i.e., standard deviation, σ) of
276 the NO₂ and NO₃ measurements were ± 80 pptv and ± 3 pptv (1 s data), respectively. For the
277 NO₃ channels, additional noise was introduced by variable background absorption of NO₂,
278 O₃, and water vapor which produce small, spurious structure in the 662 nm absorption signal
279 (Dubé et al., 2006) and were not tracked well by the interpolation of the baseline from the
280 hourly τ_0 determinations.

281 During the Abbotsford campaign, only five (four blue and one red) CRDS channels were
282 operated because of delays in the fabrication of the final set of CRDS mirror holders. The
283 662 nm CRDS cell sampled from a Teflon™ inlet heated to 130 °C for quantification of NO₃
284 plus the NO₃ generated from thermal dissociation N₂O₅ (Brown et al., 2001; Simpson, 2003;
285 Dubé et al., 2006). Under the high-NO_x conditions of this study, equilibrium (2) was
286 sufficiently far to the right (see section 3.3) such that $[\text{NO}_3] + [\text{N}_2\text{O}_5] \approx [\text{N}_2\text{O}_5]$, i.e., the
287 concentration measured could be equated with $[\text{N}_2\text{O}_5]$ without introducing a large error (i.e.,
288 <5%). The four 405 nm CRDS cells were operated as follows: The first sampled from an
289 ambient temperature inlet and was used to quantify NO₂. The second sampled from a quartz
290 inlet heated to 250 °C and was used to quantify NO₂ plus total peroxyacyl nitrate (Σ PAN)
291 (Paul et al., 2009; Paul and Osthoff, 2010). Data from this channel will be presented in a
292 future manuscript. The third was operated with a quartz inlet heated to 450 °C to enable
293 ClNO₂ calibrations (Thaler et al., 2011). Quantification of total alkyl nitrates (Σ AN) in
294 ambient air was not attempted because of the high NO_x levels and resulting large subtraction
295 errors (Thieser et al., 2016). The fourth 405 nm CRDS cell was connected with polycarbonate
296 tubing ($\frac{3}{8}$ " o.d. and $\frac{1}{4}$ " i.d.) in series to the 662 nm channel and was used to calibrate the
297 response of the N₂O₅ channel, which is a function of the transmission efficiency of N₂O₅
298 through the inlet and the overlap of the diode laser spectrum with the NO₃ absorption line
299 (Odame-Ankrah and Osthoff, 2011). The role of the polycarbonate tube was to scrub NO₃
300 exiting the N₂O₅ channel, allowing detection of only the NO₂ generated from thermal

301 dissociation of N_2O_5 and to prevent recombination of NO_3 and NO_2 in the blue calibration
302 channel (Wagner et al., 2011).

303 N_2O_5 was generated in situ by adding an excess of O_3 (generated by passing O_2 past a 254 nm
304 Hg lamp) to nitric oxide (NO) in a 0.635 cm (1/4") o.d. and 0.476 cm (3/16") i.d. Teflon™
305 calibration line and allowed to equilibrate (i.e., until the output was constant) offline before
306 being switched inline on demand. The N_2O_5 response (which accounted for N_2O_5 loss in the
307 sampling line and slight mismatches of the laser wavelengths with the NO_3 absorption line)
308 varied between 65% and 100% and depended on inlet "age"; the Teflon™ inlet and aerosol
309 inlet filter were changed every 2 – 3 days. The accuracy of the NO_2 and N_2O_5 data were $\pm 10\%$
310 and $\pm 25\%$, respectively, driven mainly by the systematic uncertainty of the NO_2 absorption
311 cross-section and of the N_2O_5 inlet transmission efficiency (Odame-Ankrah, 2015).

312

313 2.2.3 Measurements of O_3 , NO and NO_y ,

314 Mixing ratios of O_3 were monitored by UV absorption in a commercial instrument (Thermo
315 49) and were accurate within $\pm 2\%$ and ± 1 ppbv. An NO-O_3 chemiluminescence instrument
316 (Thermo 42i) was used to monitor mixing ratios of NO and NO_y , which was reduced to NO in
317 a Mo converter heated to ~ 320 °C placed outside a short distance (~ 1 m) from the sample
318 inlet. This instrument sampled from the main inlet via a Teflon™ filter and filter holder and
319 was calibrated daily against CRDS as described by Tokarek et al. (2014). The slope
320 uncertainty for each multipoint calibration was $\pm 15\%$. Interpolation between calibration runs
321 gave an overall uncertainty of $\pm 30\%$. The NO zero offset uncertainty (needed for calculating
322 the NO_3 loss rate with respect to reaction with NO , R9) was ± 10 pptv.

323

324 2.2.4 VOC measurements

325 Volatile organic compounds were monitored with a commercial gas chromatograph - mass
326 spectrometer (GC-MS; Agilent model 7890A and 5975C) equipped with an FID detector and
327 a Markes Unity 2 pre-concentrator with an ozone precursor trap cooled to -25 °C.

328 In a typical sampling sequence, a 500 mL air sample was collected at a flow rate of 25 mL
329 min^{-1} , taken from the center flow of a 1.27 cm (1/2") stainless steel inlet line which was
330 continuously sampling ambient air at 5 L min^{-1} . The sampled air flowed through a 0.318 cm

331 (1/8") stainless steel line and particles were removed using a 1 μm pore size fritted filter.
332 Once 500 mL of air were collected, the pre-concentrator was flushed with helium to remove
333 air while awaiting injection. At the start of a GC run, the sample in the pre-concentrator was
334 flash heated to 300 °C and held for 3 min. The sample was separated on 2 columns with the
335 entire sample going through the Agilent VRX column with a Dean switch directing the first
336 gases emitted to a second GasPro column and then to the FID detector ($\sim < \text{C}_4$) while the
337 heavier compounds were detected using the MS detector in scan mode.

338 The cycle time for the GC analysis was 1 hour with the sample being collected during the
339 previous runs analyses. The 20 min sample was taken at the start of a 1 hour time period.

340 Due to the low temperature of the trap, the air was dried using a trap at -30 °C. The trap was
341 heated and dried between each sample and reconditioned for 10 min prior to sample
342 collection. All sample lines were stainless steel with a Restek SulfinertTM coating to minimize
343 sample loss on the lines. Calibrations were performed once per day for 105 species using a
344 100 ppbv U.S. Environmental Protection Agency (EPA) photochemical assessment
345 monitoring system (PAMS) and a 100 ppb EPA air method, toxic organics – 15 (TO15)
346 standard tanks (Linde Specialty Gases) at an approximately concentration of 2 ppbv. The
347 terpenes were semi-quantitatively measured as a calibration source was not available at the
348 time and only the changes in concentration strength with time of day were used. The accuracy
349 of the measurements varied depending on the species but was better than $\pm 30\%$ throughout.
350 Peaks were manually reintegrated using Chemstation software from Agilent. Table S-1
351 summarizes the VOCs quantified.

352

353 **2.3 Aerosol measurements**

354 The chemical composition of non-refractory PM_{10} was monitored using an Aerosol Chemical
355 Speciation Monitor (ACSM, Aerodyne), which reported concentrations of NO_3^- , SO_4^{2-} , Cl^- ,
356 NH_4^+ , and total organics. A general description of this instrument designed for routine
357 monitoring has been given by Ng et al. (2011). The composition of the refractory aerosol (i.e.,
358 sea salt) was not quantified.

359 Submicron aerosol size distributions were quantified by a scanning mobility particle sizer
360 (SMPS, TSI 3034). This instrument measured aerosol particles in the range from 10 to 487
361 nm using 54 size channels (32 channels per decade). Both of these instruments were housed in

362 a trailer operated by Metro Vancouver. The ACSM and the SMPS sampled air off a shared
363 stainless steel inlet that had a total flow of 5 L min^{-1} and contained a $\text{PM}_{2.5}$ sharpcut filter at
364 the inlet and was operated at ambient relative humidity.

365

366 **2.4 Photolysis frequencies**

367 Photolysis frequencies were determined by solar actinic flux spectroradiometry
368 (Hofzumahaus et al., 1999) using a commercial radiometer with 2π receptor optics and photo
369 diode array (PDA) detector (Metcon; 512 pixels, wavelength range 285 nm - 690 nm)
370 calibrated by the manufacturer. The spectrometer was mounted facing up (zenith view) and
371 hence measured the down-welling radiation. On several days, the spectrometer was inverted
372 hourly to determine the up-welling radiation, which was added to the down-welling flux.
373 Photolysis frequencies including $j(\text{NO}_3)$, $j(\text{NO}_2)$, $j(\text{O}^1\text{D})$, and $j(\text{ClNO}_2)$ were calculated using
374 reference spectra and quantum yields from (Sander et al., 2010) and (Ghosh et al., 2012).
375 Table 2 gives the ratio of observed up-welling to down-welling for selected photolysis
376 frequencies. For August 3 (a cloud-free day), the measurements were compared to (hourly)
377 predictions with the online "Tropospheric Ultraviolet and Visible (TUV) Radiation Model"
378 V5.0 (Madronich and Flocke, 1997); with default settings, the model reproduced the
379 measured $j(\text{NO}_2)$ and $j(\text{O}^1\text{D})$ quite well: a scatter plot of observed against TUV rate constants
380 had correlation coefficients (r) of 0.997 and 0.998, slopes of 1.06 ± 0.02 and 1.10 ± 0.02 , and
381 offsets of $(3 \pm 1) \times 10^{-4} \text{ s}^{-1}$ and $(5 \pm 3) \times 10^{-7} \text{ s}^{-1}$.

382 **2.5 Box model simulations of the nocturnal O_3 and O_x loss in the NBL**

383 A box model was set up to reconcile the median nocturnal decays of O_3 and O_x . These
384 simulations are intended as back-of-the-envelope type estimates of major processes only since
385 an accurate description of the nocturnal boundary layer chemistry would require modeling of
386 horizontal and vertical transport, i.e., altitude-resolved information not available in this study
387 (Geyer and Stutz, 2004). The model's assumptions are a well-mixed NBL that is decoupled
388 from the NRL above it as observed by earlier balloon vertical profiling (Pisano et al., 1997),
389 O_3 and NO_2 dry deposition velocities of $v_d(\text{O}_3) = 0.2 \text{ cm s}^{-1}$ and $v_d(\text{NO}_2) = \alpha v_d(\text{O}_3)$ with
390 $\alpha = 0.65$ (Lin et al., 2010), and negligible chemical O_3 and O_x losses other than titration of O_3
391 by NO (R8) and by reaction with a generic biogenic hydrocarbon (assumed to react with O_3

392 with a rate coefficient of $5 \times 10^{-11} \text{ cm}^3 \text{ molec.}^{-1} \text{ s}^{-1}$, i.e., the rate coefficient for reaction of α -
393 pinene with O_3 (Seinfeld and Pandis, 2006)). Simulations were initiated with the median NO_2
394 and O_3 concentrations observed at sunset. More details are given in the S.I.

395

396 **3 Results**

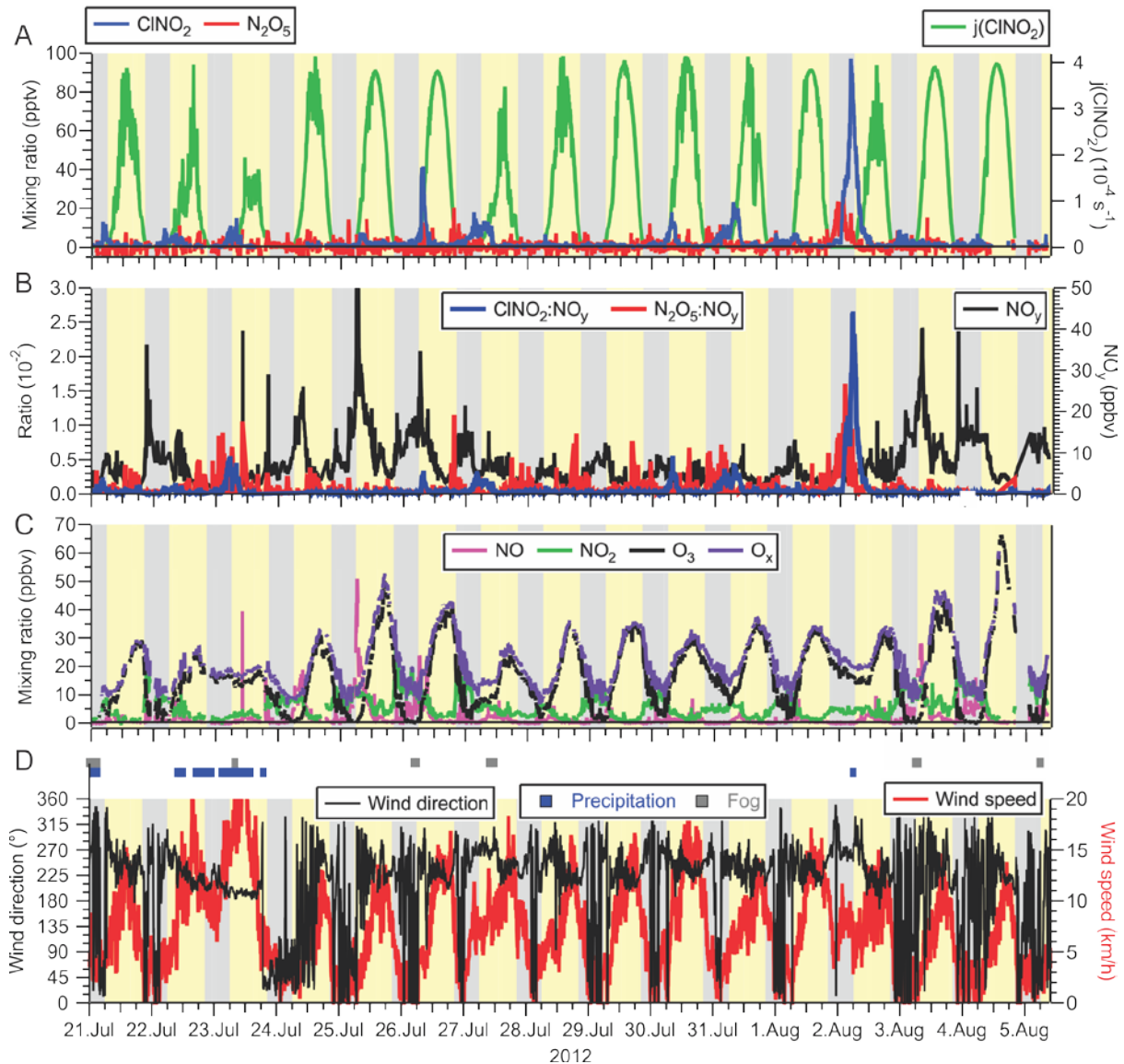
397 **3.1 Overview of data set**

398 **3.1.1 Meteorology**

399 A time series of local wind direction and speed are displayed in Figure 3D. During the two-
400 week long measurement period, the air flow to the site was from the Pacific Ocean to the SW
401 and WSW with a moderate wind speed of 8.7 km hr^{-1} (median value). On most nights, local
402 wind speeds were calm, i.e., $< 5 \text{ km hr}^{-1}$ (median speed 3.6 km hr^{-1}) and from variable
403 directions, though predominantly from the W and N. The two exceptions were the nights of
404 July 22/23 and August 1/2 when stronger winds ($> 5 \text{ km hr}^{-1}$) from the W and SW persisted.
405 These nights saw relatively high ClNO_2 mixing ratios (see section 3.1.4).

406 The air temperatures were quite mild and ranged from a minimum of $11.0 \text{ }^\circ\text{C}$ to a maximum
407 of $31.9 \text{ }^\circ\text{C}$. The warm temperatures shifted equilibrium K_2 from N_2O_5 towards NO_3 and NO_2
408 (further analyzed in section 3.2.2). At night, temperatures frequently dropped to the dew
409 point, resulting in occasional fog formation (shown as grey rectangles in Figure 3D),
410 sometimes after sunrise. Fog droplets are strong sinks for N_2O_5 (Osthoff et al., 2006). In total,
411 the impact of fog was minor, affecting 5% of the data. In addition, there were two periods
412 with precipitation: The first occurred intermittently on July 20 until the morning of July 21.
413 The second rainfall event was a 24-hour period from mid-day July 22 to the afternoon of July
414 23 (shown as blue dots in Figure 3D). July 23 also exhibited the highest wind speeds of the
415 campaign (Figure 3C) and lowest daytime photolysis frequencies. The time series of $j(\text{ClNO}_2)$
416 is shown as a representative example in Figure 3A. The photolysis data indicates that it was
417 sunny on 6 days (July 25, 26, 29, Aug 1, 4 and 5) and that the remaining days had variable
418 cloud cover, consistent with hourly meteorological logs that showed 10% of the measurement
419 period affected by precipitation.

420



422

423 **Figure 3.** (A) Time series of N₂O₅ and CINO₂ mixing ratios (left axis) and CINO₂ photolysis
 424 frequency (right axis) observed at T45 near the Abbotsford International Airport. (B) Time
 425 series of the ratios of CINO₂ and N₂O₅ to NO_y (left axis) and of NO_y (right axis). (C) Time
 426 series of NO, NO₂, O₃, and O_x (= NO₂ + O₃) mixing ratios. (D) Time series of local wind
 427 direction (left axis) and speed (right axis). The blue and grey dots above the time series
 428 indicates periods of precipitation (drizzle or rain) and fog, respectively, as identified in hourly
 429 meteorological logs.

430

431 3.1.2 NO and NO₂

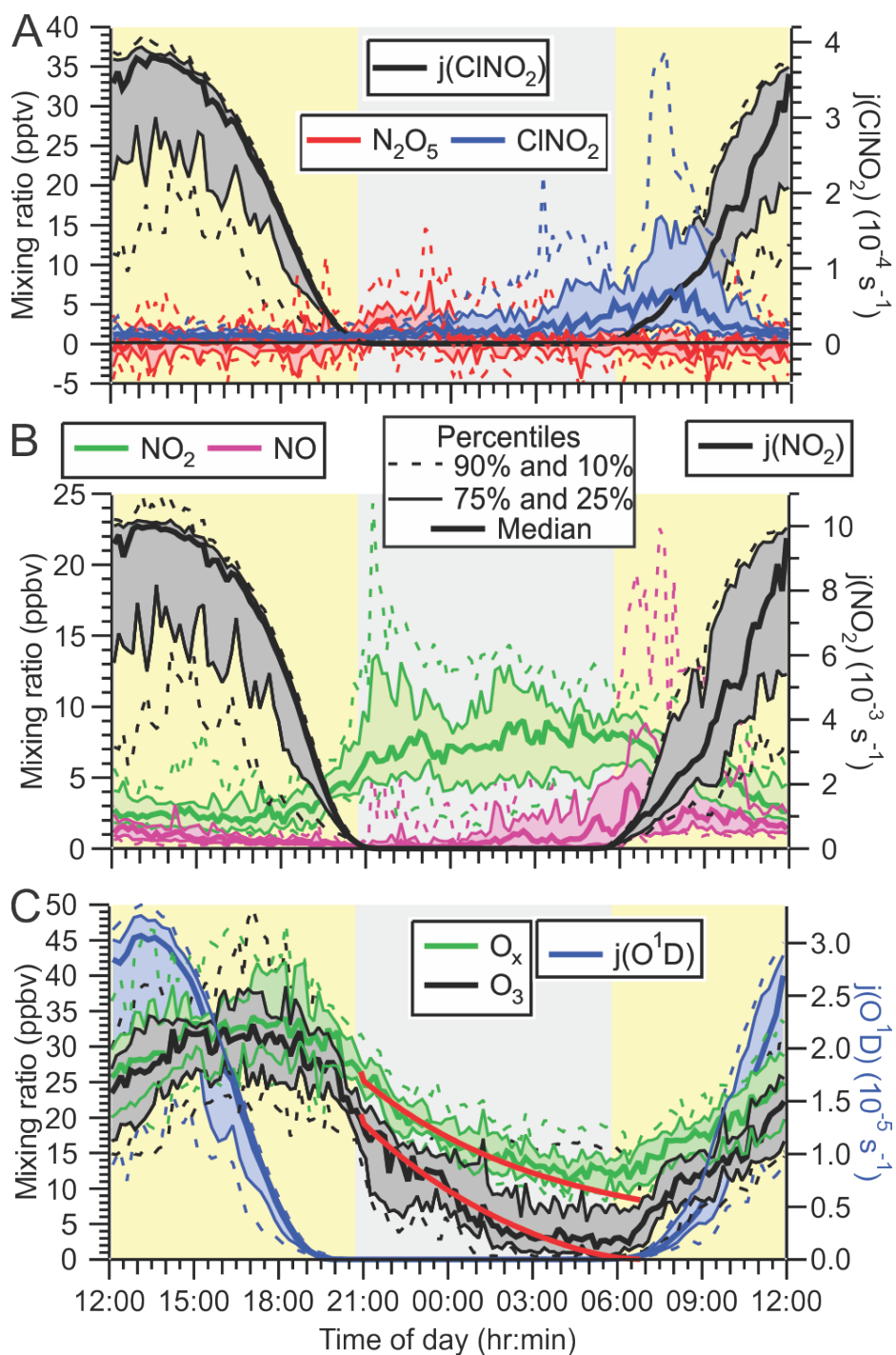
432 The rates of N₂O₅ and ClNO₂ formation depend on the rate of NO₃ production,
433 $P(\text{NO}_3)=k_1[\text{NO}_2][\text{O}_3]$ (analyzed further in section 3.2.2); therefore, it is informative to first
434 examine the mixing ratios of NO₂ and O₃ (see section 3.1.3). The time series of NO, NO₂, O₃,
435 and O_x (= O₃ + NO₂) mixing ratios are shown in Figure 3C, and their diurnal averages are
436 shown as 10th, 25th, 50th, 75th and 90th percentiles in Figures 4B and 4C.

437 The median NO and NO₂ mixing ratios for the entire campaign were 0.9 and 5.9 ppbv,
438 respectively. The average NO_x/NO_y ratio for the entire campaign was 0.9±0.4. These
439 concentration levels are characteristic of an urban air mass impacted by relatively fresh
440 emissions from combustion engines in automobiles.

441 At night, mixing ratios of NO were generally lower than during the day though not negligible
442 (median 0.3 ppbv, Figure 4B) as NO was oxidized by O₃ to NO₂ (R8) and was not replenished
443 by NO₂ photolysis. However, mixing ratios of NO increased throughout the night, often
444 coinciding with complete nocturnal removal of O₃ (see section 3.1.3), which indicates the
445 presence of nearby combustion sources of NO_x (most likely automobile exhaust). The
446 presence of NO titrates NO₃ (R3) and effectively shut down N₂O₅ and ClNO₂ production for
447 most of the study: 68% of the measurement period had NO mixing ratios > 100 pptv and NO₃
448 lifetimes (with respect to its reaction with NO) of < 15 s. In contrast, NO₂ mixing ratios were
449 highest at night (median 7.3 ppbv), amplified further by NO_x emissions that continued
450 throughout the night and likely by low nocturnal mixing heights (see discussion).

451 Mixing ratios of NO and NO_x were highest in the morning hours. Concentration changes at
452 this time of day are difficult to interpret since the NBL breaks up during this time, resulting in
453 vertical mixing of air masses, photolabile species (e.g., ClNO₂, HONO, N₂O₅, etc.) that
454 accumulated overnight begin to photodissociate, and local emissions change with the onset of
455 rush hour.

456 In contrast to the morning increase in NO, an afternoon/early evening maximum in NO was
457 absent. This can be rationalized by a greater abundance of oxidants that oxidize NO to NO₂,
458 i.e., O₃ (see Figures 3 and 4 and section 3.1.3) and organic peroxy radicals in the afternoon, a
459 topic outside the scope of this manuscript.



460

461 **Figure 4.** (A) Diurnal variation of ClNO_2 and N_2O_5 mixing ratios (left axis) and ClNO_2
 462 photolysis frequencies (right axis). (B) Diurnal profiles of NO and NO_2 (left axis) and NO_2
 463 photolysis frequency (right axis). (C) Diurnal profiles of O_3 and $\text{O}_x = \text{O}_3 + \text{NO}_2$ (left axis) and
 464 $\text{O}_3 \rightarrow \text{O}(^1\text{D})$ photolysis frequency (right axis). The superimposed lines shown in red are results
 465 from a simple box model (see text).

466

467 3.1.3 O₃ and O_x

468 The time series of O₃ mixing ratios and its diurnal profile are shown in Figure 3C and 4C,
469 respectively. O₃ mixing ratios were small (average ± 1 standard deviation of 16 ± 12 ppbv) and
470 peaked at $\sim 17:00$ in the afternoon. The highest concentrations were observed on August 4
471 from 13:55 to 15:30, when mixing ratios were 64 ± 1 ppbv (the 8-hour running average was 52
472 ppbv). These levels were well below the CAAQS 8-hr standard of 63 ppbv and the 1 hour
473 National Ambient Air Quality Objective of 82 ppbv, smaller than the pre-2003 data analyzed
474 by Ainslie and Steyn (2007), who reported between 10 and 20 O₃ 1-hour exceedences of 82
475 ppbv in the 1980s, and of similar magnitude as observed by a high-density monitoring
476 network in the region in 2012 (Bart et al., 2014), which observed peak O₃ levels of 74 and 83
477 ppbv at Abbotsford on July 8 and August 17, respectively.

478 A recurring feature of this data set was the rapid and often complete loss of O₃ at night
479 (Figure 4C). This was accompanied by an increase in the NO₂ mixing ratios, though by less
480 (+6 ppbv on average) than the amount of O₃ that was lost (-26 ppbv on average), showing that
481 NO to NO₂ conversion (R8) was a contributor, though minor ($\sim 25\%$) to the nocturnal O₃ loss.

482 The diurnal profile of O_x was similar to that of O₃, in that the highest concentrations occurred
483 in the afternoon (at $\sim 18:00$) and a considerable fraction of O_x was removed at night. At
484 sunset, a median amount of 26 ppbv of O_x were present, which decreased to 12 ppbv at
485 sunrise (Figure 4C). The pathways contributing to nocturnal O₃ and O_x loss are probed using
486 box model simulations in section 3.2.1.

487 There were two (out of 16 total) nights when O₃ was not completely removed. On July 22-23
488 and August 1-2, O₃ mixing ratios dropped from a daytime maxima of ~ 33 ppbv to non-zero
489 nocturnal minima of ~ 16 ppbv. On both of these nights, ClNO₂ and N₂O₅ mixing ratios were
490 elevated (Figure 3A), and the two largest ClNO₂ to NO_y ratios were observed (Figure 3B).
491 The local wind speeds were > 6 km hr⁻¹, whereas on other nights, local winds were calmer
492 (Figure 3C). The greater local wind speeds likely induced more turbulence and a higher
493 vertical mixing height.

494

495 3.1.4 N₂O₅ and ClNO₂

496 Time series of ClNO₂ and N₂O₅ mixing ratios and ClNO₂ photolysis frequencies are shown in
497 Figure 3A. Mixing ratios of ClNO₂ and N₂O₅ were small (campaign averages at night of
498 4.0 pptv and 1.4 pptv, respectively). The mixing ratios peaked prior to sunrise at median
499 values of 7.9 and 7.8 pptv for ClNO₂ and N₂O₅, respectively. The highest mixing ratios of this
500 campaign were 97 pptv for ClNO₂ and 23 pptv for N₂O₅, both observed on the night of
501 August 1-2. This night was also the only time when nocturnal ClNO₂ mixing ratios exceeded
502 20 pptv and is analyzed in greater detail in section 3.2.3.

503 Consistent with their low mixing ratios, neither ClNO₂ nor N₂O₅ were significant components
504 of NO_y (Figure 3B): on average, they contributed 0.1% to the nocturnal NO_y budget, though
505 NO_y mixing ratios were large (median 6.3 ppbv at night), typical for a site impacted by urban
506 emissions. The only exception was the night of August 1-2, when ClNO₂ and N₂O₅
507 constituted 2.6% and 1.6% of NO_y, respectively, and NO_y mixing ratios were 4.4 ppbv on
508 average (Figure 3B).

509 The ClNO₂ and N₂O₅ mixing ratios are displayed as functions of time of day in Figure 4A.
510 Before midnight local time, N₂O₅ mixing ratios were slightly larger (median value of 1.8 pptv
511 on average) than those of ClNO₂ (median value of 1.4 pptv on average), whereas after
512 midnight, ClNO₂ mixing ratios were larger than those of N₂O₅ (2.0 pptv vs. 0.6 pptv). The
513 latter is consistent with observations at other ground sites, which generally showed higher
514 concentrations of the longer-lived ClNO₂ prior to sunset (Thornton et al., 2010; Mielke et al.,
515 2013). The higher N₂O₅ than ClNO₂ abundances at the beginning of the nights suggests that
516 the N₂O₅ production rate at that time exceeded its ability to react heterogeneously and convert
517 to ClNO₂, potentially due to a lack of available aerosol chloride or otherwise reduced N₂O₅
518 heterogeneous uptake parameters (Thornton et al., 2010).

519 Production of ClNO₂ from N₂O₅ uptake on aerosol ceases after sunrise because of the rapid
520 removal of N₂O₅ and NO₃ as the latter is titrated by NO and destroyed by photolysis (R3 and
521 R4) (Wayne et al., 1991). In spite of this, ClNO₂ mixing ratios frequently (on 12 out of 15
522 measurement days) continued to increase after sunrise (Figures 3A and 4), peaking on average
523 at ~07:45 in the morning approximately 2 hours after sunrise. The median mixing ratio at that
524 time was 6.7 pptv larger than the median value of 5.3 pptv observed at sunrise. The most
525 prominent example of this phenomenon occurred on the morning of July 26. For a two hour
526 period leading up to sunrise, there was fog (virtually ensuring the absence of N₂O₅), and

527 ClNO₂ mixing ratios were < 5 pptv. The fog then dissipated at sunrise. One hour later, ClNO₂
528 mixing ratios increased to > 40 pptv. Similar events (though with more modest ClNO₂
529 increases) were observed on the mornings of July 22, 23, 25, 27, 28, 30, 31, and Aug 1. Two
530 of these (July 23 and 27) overlapped with brief fog events.

531 Qualitatively similar ClNO₂ morning peaks have been observed at other ground sites and
532 were rationalized by vertical mixing (Tham et al., 2016; Bannan et al., 2015; Faxon et al.,
533 2015).

534 In the period after the ClNO₂ morning peak after ~09:00, ClNO₂ mixing ratios decreased,
535 coinciding with the increasing ClNO₂ photolysis rate. Box model simulations (see S.I.)
536 indicate that the decay of ClNO₂ (after 09:00) was consistent with its destruction by
537 photolysis.

538 There were two exceptions: the mornings of July 27 and Aug 2, when the decay of ClNO₂
539 concentration occurred at a rate faster than its photolysis. On July 27, fog was not observed
540 until 8:00, at which time the ClNO₂ mixing ratio rapidly decreased because of dissolution
541 and/or an air mass shift to one with a different chemical history. On Aug 2, the campaign
542 maximum of 97 pptv was observed at 04:40 prior to sunrise, followed by a sharp decline.
543 Hourly logs indicated scattered showers at 06:00.

544

545 3.1.5 PM₁ size distribution and composition measurements

546 The time series of PM₁ surface area density (S_A) observed by the SMPS is shown in Figure
547 5A. The aerosol loadings were modest: the average (median) surface area density was 128
548 (104) μm² cm⁻³ and ranged from extremes of 26 to 618 μm² cm⁻³. The size distribution data
549 show that bulk of the surface area (i.e., the mean diameter (\bar{D}_s)) is in the range of 200 to 300
550 nm, such that most of the area of the accumulation mode was captured. However, the surface
551 area calculations do not include contributions from larger diameter particles which were not
552 quantified. Shown on the right hand side of Figure 5A is the rate coefficient for heterogeneous
553 uptake of N₂O₅, k_{N₂O₅} calculated using equation (1).

$$554 \quad k_{\text{N}_2\text{O}_5} = \frac{1}{4} \gamma \bar{c} S_A \quad (1)$$

555 Here, γ and \bar{c} are the uptake probability and the mean molecular speed of N₂O₅, respectively.
556 Equation (1) is valid for uptake on small, submicron aerosol as it neglects gas-phase diffusion

557 limitations (Davidovits et al., 2006). For this calculation, a γ value of 0.025 was assumed. The
558 average (± 1 standard deviation) of $k_{\text{N}_2\text{O}_5}$ was $(2\pm 1)\times 10^{-4} \text{ s}^{-1}$.

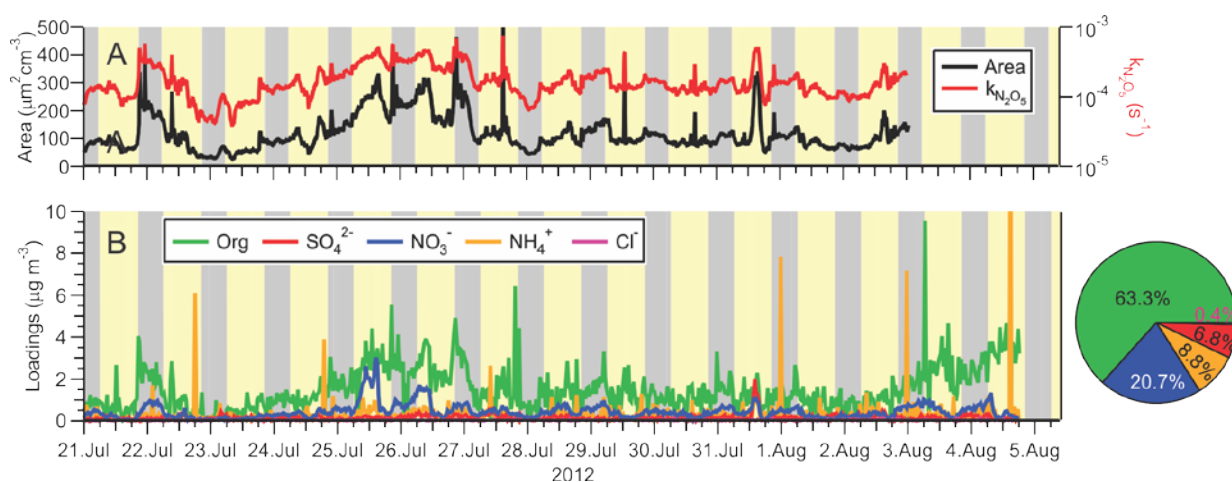
559 The ACSM submicron aerosol composition data are shown as a time series in Figure 5B and
560 as a function of time of day in Figure 6. Consistent with the size distributions, mass loadings
561 were also modest overall (average $2.3 \mu\text{g m}^{-3}$). The ACSM factor analysis identified
562 oxygenated organic aerosol (OOA) as the largest mass fraction of the non-refractory aerosol
563 (average \pm standard deviation $1.4\pm 1.2 \mu\text{g m}^{-3}$, 63.3% of the total aerosol mass measured by
564 the ACSM). Hydrocarbon-like organic aerosol (HOA) associated with primary emissions was
565 a minor component (average $0.03 \mu\text{g m}^{-3}$, 1.1%) but occasionally enhanced in plumes
566 (maximum $8.3 \mu\text{g m}^{-3}$). The oxygenated aerosol fraction (OOA) did not exhibit a discernible
567 diurnal profile (Figure 6A), which is consistent with the modest photochemistry at this site as
568 judged from the modest peak O_3 levels observed. The inorganic mass fraction was dominated
569 by nitrate ($0.47\pm 0.40 \mu\text{g m}^{-3}$, 20.7%). The second most abundant inorganic component was
570 ammonium ($0.2\pm 1.4 \mu\text{g m}^{-3}$, 8.8%) followed by sulfate ($0.15\pm 0.15 \mu\text{g m}^{-3}$, 6.8%). The data
571 are of similar magnitude as aerosol mass spectrometry (AMS) data collected at nearby
572 Langley as part of Pacific 2001 (Boudries et al., 2004); then, organics had also been the
573 largest component (average of $1.6 \mu\text{g m}^{-3}$, 49%), though sulfate and ammonium mass loadings
574 had been larger (0.88 and $0.44 \mu\text{g m}^{-3}$, 25% and 14%, respectively) and nitrate mass loadings
575 smaller ($0.38 \mu\text{g m}^{-3}$, 12%).

576 The neutralization ratio, $\text{NR} \approx [\text{NH}_4^+]:([\text{NO}_3^-]+2[\text{SO}_4^{2-}])$ (Zhang et al., 2007), where the
577 square brackets denote molar concentrations (calculated from the mass concentrations
578 reported by the ACSM by dividing by the appropriate molecular weights), was 1.19 (median
579 value). The high NH_3 content is qualitatively consistent with the non-quantitative data
580 collected by Metro Vancouver (using a Thermo Scientific 17i $\text{NH}_3/\text{NO}/\text{NO}_2/\text{NO}_x$ analyzer),
581 which showed large concentrations of gas-phase NH_3 (Figure S-1).

582 The ACSM software also reported non-refractory chloride with an average (± 1 standard
583 deviation) concentration of $0.01\pm 0.03 \mu\text{g m}^{-3}$, though it is unclear if this signal was real as it
584 did not vary over the course of the campaign and was below the stated ACSM detection of
585 limit of $0.2 \mu\text{g m}^{-3}$ (Ng et al., 2011).

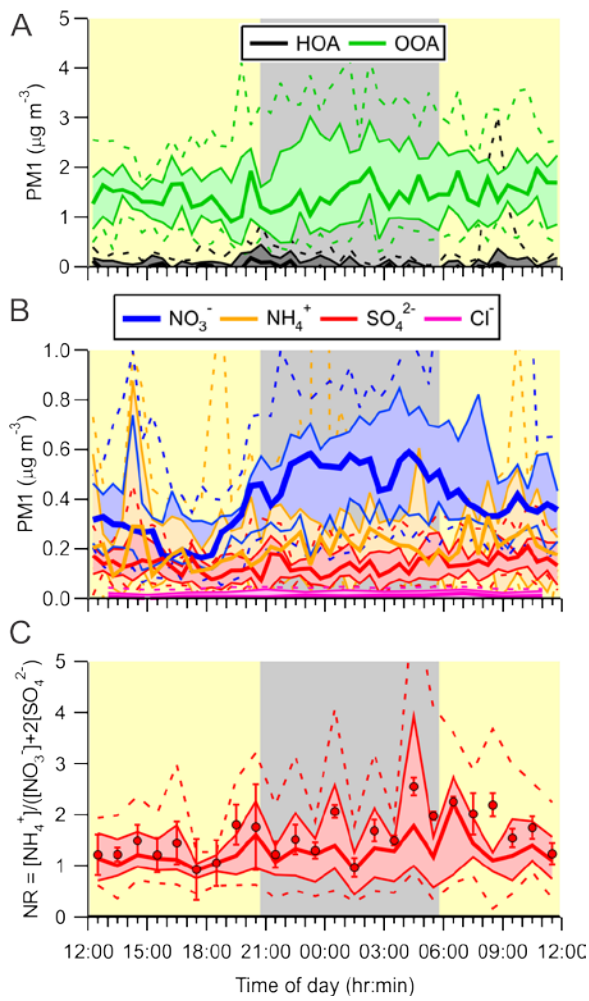
586 Aerosol nitrate exhibited a clear diurnal profile with higher concentrations at night (Figure
587 6B). In particular, the amount of aerosol nitrate increased at the beginning of the night, when
588 the nocturnal NO_3 production rates were greatest.

589 Previous AMS measurements in Vancouver during the month of August as part of Pacific
 590 2001 reported a slightly higher total mass loadings of $7.0 \mu\text{g m}^{-3}$ that included a greater HOA
 591 component ($2.4 \mu\text{g m}^{-3}$, 34%) and a smaller nitrate fraction ($0.6 \mu\text{g m}^{-3}$, 8.5%) (Alfarra et al.,
 592 2004; Jimenez et al., 2009) than observed here. The lower HOA in this data set are likely a
 593 result of tighter emission controls implemented since the earlier study, a topic outside the
 594 scope of this paper.
 595



596
 597 **Figure 5.** Time series of (A) submicron surface area density measured by the TSI 3034
 598 scanning mobility particle sizer (left-hand side) and calculate heterogeneous N_2O_5 uptake rate
 599 coefficient assuming $\gamma=0.025$ (right-hand side), and (B) non-refractory submicron aerosol
 600 species measured by ACSM. The average total loading was $2.3 \mu\text{g m}^{-3}$. The pie chart shows
 601 the average campaign composition.
 602

603



604

605 **Figure 6.** Diurnal averages of submicron (PM1) ACSM data. (A). Organic aerosol displayed
606 as hydrocarbon-like organic aerosol (HOA) and oxygenated organic aerosol (OOA) factors.
607 (B) Inorganic aerosol fractions. (C) Neutralization ratio (NR).

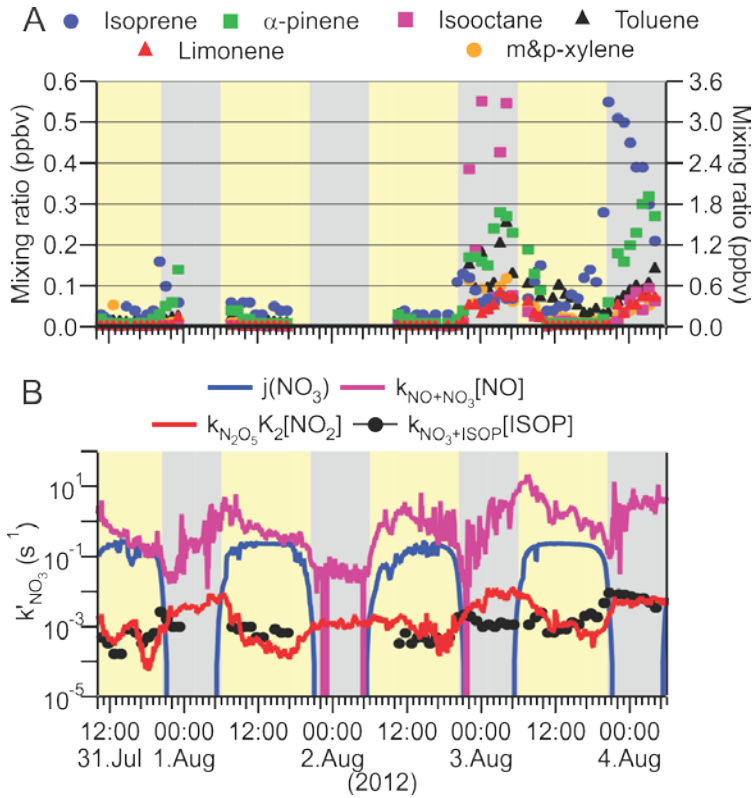
608 3.1.6 Hydrocarbon measurements

609 Mixing ratios of hydrocarbons were quantified during daytime and during the nights of
610 August 2-3 and 3-4. A portion of the hydrocarbon data is shown in Figure 7A. Mixing ratios
611 were generally smaller during the day than during night, due to the larger daytime mixing
612 heights. On the nights of August 2/3 and 3/4, N_2O_5 was not detected, consistent with low
613 $P(NO_3)$ values as O_3 mixing ratios approached zero (Figure 3). At the same time, there were
614 strong NO_3 sinks present: Mixing ratios of α -pinene and limonene (left-hand axis) increased
615 throughout the night, as thermal emissions continued into the shallow NBL. In contrast,
616 mixing ratios of isoprene, whose emissions are driven by photosynthesis (Hewitt et al., 2011;
617 Guenther et al., 1995), increased at the beginning of the nights and then decreased as isoprene
618 was removed by oxidation with O_3 and NO_3 and by transport. Throughout both nights, the site
619 was also influenced by anthropogenic hydrocarbons (e.g., isooctane and toluene, right-hand
620 axis). Because synoptic conditions as judged from local wind speed and direction (Figure 3D)
621 were similar on most of the other nights when hydrocarbons were not quantified, the data
622 shown in Figure 7A were likely representative for much of the campaign.

623 The VOC data were not sufficiently comprehensive to allow an accurate determination of the
624 NO_3 loss frequency to hydrocarbons, given by $\sum k_{NO_3+VOC,i}[VOC]_i$. Shown in Figure 7B is the
625 loss frequency of NO_3 to isoprene, calculated by multiplying its concentration with the NO_3
626 rate coefficient taken from Seinfeld and Pandis (2006). Loss of NO_3 to isoprene was a small
627 sink compared to its loss to NO via R3 and NO_3 photolysis (R4) but was approximately on
628 par with its indirect loss, i.e., the heterogeneous uptake of N_2O_5 .

629

630



631

632 **Figure 7.** (A) Time series of selected VOC mixing ratios observed on the nights of August
 633 2/3 and August 3/4, 2012. Biogenic VOCs (isoprene, α -pinene and limonene) are shown on
 634 the left-hand axis, and anthropogenic VOCs (isooctane, toluene and m&p-xylene) on the
 635 right-hand axis. The α -pinene and limonene measurements are semiquantitative. (B) Time
 636 series of NO_3 loss rate coefficients. ISOP = isoprene.

637

638 3.2 Analysis

639 3.2.1 Box model simulations of the nocturnal O₃ and O_x loss in the NBL

640 In initial simulations, the O₃ and NO₂ deposition rates were tuned until the median nocturnal
641 O_x loss was reproduced. An O₃ dry deposition rate of $4 \times 10^{-5} \text{ s}^{-1}$ produced a simulation that
642 reasonably matched the observations (Figure S-2). The magnitude of this rate corresponds to a
643 NBL height of 50 m, the same mixing height that was frequently observed in balloon vertical
644 profiles reported by Pisano et al. (1997). However, since wind speeds at night were low
645 during the study (median 3.6 km hr^{-1}), the aerodynamic resistance to vertical transport was
646 likely elevated due to reduced turbulence. It is therefore conceivable that the O₃ dry
647 deposition velocity was in actuality smaller than the values taken from Lin et al. (2010) and
648 the mixing height was greater than 50 m.

649 Modeling studies have assumed N₂O₅ and NO₃ deposition velocities of up to 2 cm s^{-1} in urban
650 areas (Sander and Crutzen, 1996); adopting this value allows the dry deposition rate constants
651 of N₂O₅ and NO₃ to be estimated at $\sim 4 \times 10^{-4} \text{ s}^{-1}$, which is on par with the estimated
652 heterogeneous uptake rate constant of N₂O₅ on submicron aerosol.

653 Next, the generic biogenic VOC was added. For this, a biogenic hydrocarbon abundance of
654 1 ppbv at sunset (mostly isoprene – see Figure 7) and a (monoterpene) emission rate of 3×10^5
655 molecules $\text{cm}^{-3} \text{ s}^{-1}$ based on the crop emission factor given by Guenther et al. (2012) into a
656 50 m deep NBL were assumed. This assumed flux gives a similar emission rate as the 0.3
657 ppbv increase over a 6 hour period observed on Aug 3-4 (Figure 7). The addition of this
658 biogenic VOC only had a marginal effect on O_x (Figure S-3).

659 The simulations presented in Figures S-2 underpredict the observed loss of O₃, necessitating
660 the addition of an NO source that results in selective removal of O₃ while preserving O_x.
661 Since automobiles are the largest NO_x source in the region, a constant emission source of 95%
662 NO and 5% NO₂ (Wild et al., 2017) was added and its magnitude varied. The NO_x source
663 strength necessary to reproduce the median O₃ loss was $\sim 1.1 \text{ ppbv hr}^{-1}$. The simulation results
664 using these parameters are superimposed (in red) in Figure 4C. There is reasonable agreement
665 between the simulations and observations of O_x and O₃ until $\sim 3:00$ (and between simulation
666 and observation of NO, Figure S-4). This shows that the nocturnal O₃ and O_x loss can be
667 rationalized without active NO₃ and N₂O₅ chemistry and suggests that NO₃, N₂O₅, and ClNO₂
668 did not contribute significantly to O_x and O₃ loss in the NBL.

669

670 3.2.2 Metrics of nocturnal nitrogen oxide chemistry: $P(\text{NO}_3)$, $\phi'(\text{ClNO}_2)$ and
671 $\tau(\text{N}_2\text{O}_5)$

672 Nocturnal N_2O_5 chemistry was analyzed using several common metrics: the rate of NO_3
673 production by R1, $P(\text{NO}_3)=k_1[\text{NO}_2][\text{O}_3]$, the yield of ClNO_2 relative to the total amount of
674 NO_3 formed at night, $\phi'(\text{ClNO}_2)$, and the steady state lifetime of N_2O_5 , $\tau(\text{N}_2\text{O}_5)$.

675 The time of day dependence of $P(\text{NO}_3)$ is shown in Figure 8A. The NO_3 production rates
676 were small (median values $< 0.3 \text{ ppbv hr}^{-1}$) and were larger during the day than at night due to
677 the low O_3 mixing ratios. After midnight, for example, the median $P(\text{NO}_3)$ was $(55\pm 23) \text{ pptv}$
678 hr^{-1} . These are very modest NO_3 production rates for a site influenced by urban emissions. In
679 a recent study on a mountain top in Hong Kong, for instance, $P(\text{NO}_3)$ in excess of 1 ppbv hr^{-1}
680 was observed in polluted air (Brown et al., 2016).

681 The median integrated nocturnal NO_3 production over the course of the night was 940 pptv
682 (Figure 8A, right hand axis), of which 600 pptv were produced before midnight. The amount
683 of ClNO_2 produced relative to this amount, $\phi'(\text{ClNO}_2)$, was very small (median 0.17% ,
684 maximum 5.4% on the morning of August 2) and considerably less than reported by our
685 group for Calgary (median 1.0%) (Mielke et al., 2016) and Pasadena, CA (median 12%)
686 (Mielke et al., 2013).

687 A frequently calculated metric of nighttime nitrogen oxide chemistry is the steady state
688 lifetimes of NO_3 and N_2O_5 , $\tau(\text{NO}_3)$ and $\tau(\text{N}_2\text{O}_5)$ (Aldener et al., 2006; Heintz et al., 1996).
689 The latter is calculated from (Brown et al., 2003; Brown and Stutz, 2012):

690
$$\tau(\text{N}_2\text{O}_5) = \frac{[\text{N}_2\text{O}_5]}{P(\text{NO}_3)} = \frac{[\text{N}_2\text{O}_5]}{k_1[\text{NO}_2][\text{O}_3]} \approx \left(k_{\text{N}_2\text{O}_5} + \frac{k_{\text{NO}_3}}{K_2[\text{NO}_2]} \right)^{-1} \quad (2)$$

691 Here, $k_{\text{N}_2\text{O}_5}$ and k_{NO_3} are the pseudo-first order loss-rate coefficients of N_2O_5 and NO_3
692 respectively, and K_2 is the equilibrium constant for equilibrium (R2).

693 A central assumption in this derivation is that NO_3 , NO_2 , and N_2O_5 more rapidly equilibrate
694 than NO_3 is formed and either NO_3 or N_2O_5 are destroyed, i.e., $\text{NO}_3+\text{N}_2\text{O}_5$ are assumed to be
695 in steady state with respect to production and loss. Brown et al. (2003) outlined potential
696 pitfalls concerning the validity of the steady state approximation and recommended that box

697 model simulations are carried out to evaluate if a steady state in N_2O_5 can be assumed. Using
 698 the median nocturnal NO_2 and O_3 mixing ratios of 7.5 ppbv and 18 to 5.0 ppbv, respectively,
 699 a temperature of 286 K, and assumed N_2O_5 and NO_3 pseudo-first order loss frequencies of
 700 $1 \times 10^{-3} \text{ s}^{-1}$ and between $1 \times 10^{-2} \text{ s}^{-1}$ and 0 s^{-1} , the time to achieve steady state in N_2O_5 is 70 min
 701 or less (see S.I.). Thus, the steady state assumption is reasonable for this data set.

702 A key parameter in equation ((2) is the strongly temperature dependent equilibrium constant
 703 K_2 (Osthoff et al., 2007). At night, the air temperatures during this study were quite warm
 704 (median nocturnal minimum of +13 °C) and did not vary a lot between nights (Figure 8B).
 705 The warm temperatures shift equilibrium R2 away from N_2O_5 and towards NO_3 and NO_2 ,
 706 making losses via NO_3 (R3-R4 and R7) more competitive with the losses of N_2O_5 (that

707 produce $ClNO_2$; R), i.e., the $\frac{k_{NO_3}}{K_2[NO_2]}$ term in equation 11 becomes large relative to $k_{N_2O_5}$.

708 On the other hand, the relatively high NO_2 mixing ratios (median value 7.5 ± 0.8 ppbv) shift
 709 the equilibrium towards N_2O_5 . Thus, in spite of the relatively warm temperatures, the
 710 $N_2O_5:NO_3$ equilibrium ratios were large on aggregate (>15 ; Figure 8B), enabling $ClNO_2$
 711 formation via R5.

712 The steady state lifetime of N_2O_5 , $\tau(N_2O_5)$, is shown as a diurnal average in Figure 8C. The
 713 median $\tau(N_2O_5)$ at night was short (~ 1 min), and the 90th percentile peaked at a modest
 714 7.6 min at sunrise, considerably shorter than observed above the NBL (Brown et al., 2006b)
 715 and at other ground sites (Wood et al., 2005; Crowley et al., 2010; Brown et al., 2016)

716 Superimposed on the right-hand side of Figure 8C are upper limits to the steady state lifetime
 717 of N_2O_5 , calculated using the sum of pseudo first-order rate coefficients for the titration of
 718 NO_3 by NO ($k_3[NO]$, R3), NO_3 photolysis ($j(NO_3)$, R4), and NO_3 dry deposition ($k_{dep}(NO_3)$),
 719 all divided by the N_2O_5 over NO_3 ratio at equilibrium given by K_2NO_2 (Figure 8B), plus the
 720 pseudo first-order rate coefficient for N_2O_5 heterogeneous uptake ($k_{het}(N_2O_5)$, equation (1))
 721 plus N_2O_5 dry deposition ($k_{dep}(N_2O_5)$).

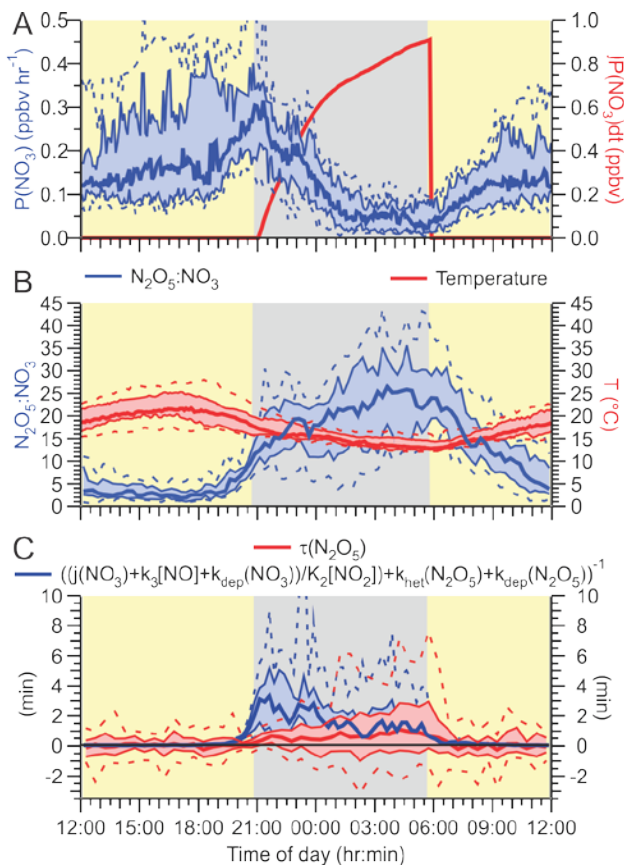
$$722 \quad \tau(N_2O_5) = \left(\frac{k_{NO_3}}{K_2[NO_2]} + k_{N_2O_5} \right)^{-1}$$

$$723 \quad < \left(\frac{k_3[NO] + j(NO_3) + k_{dep}(NO_3)}{K_2[NO_2]} + k_{het}(N_2O_5) + k_{dep}(N_2O_5) \right)^{-1}$$

724 (3)

725 The dry deposition rate constants were set to $4 \times 10^{-4} \text{ s}^{-1}$ (see section 3.2.1), which likely
 726 overestimates dry deposition during the day due to higher mixing heights; however, the error
 727 this introduces is negligible compared to the large daytime sinks such as NO_3 photolysis and
 728 its reaction with NO . Missing from equation (3) are losses of NO_3 to hydrocarbons (which
 729 were omitted because of the poor VOC data coverage) and terms for NO_3 and N_2O_5 wet (i.e.,
 730 on cloud and rain droplets) deposition. Periods affected by precipitation or fog (shown in
 731 Figure 3D) were hence excluded from the calculation. Estimates of how loss of NO_3 to VOCs
 732 could affect the lifetime of N_2O_5 are given in the S.I.

733



734

735 **Figure 8.** (A) NO_3 production rate $P(\text{NO}_3) = k_1[\text{NO}_2][\text{O}_3]$ as a function of time of day. The
 736 red line is the total amount NO_3 generated since sunset, $\int P(\text{NO}_3) dt$. (B) Equilibrium ratio of
 737 N_2O_5 to NO_3 calculated by multiplying the temperature-dependent equilibrium constant, K_2 ,
 738 with the NO_2 concentration, $[\text{NO}_2]$ (left axis), and air temperature (right axis). (C) Steady
 739 state lifetime of N_2O_5 (left axis) and upper limits calculated using equation (3) (right axis) as
 740 functions of time of day.

741

742 The median "observed" $\tau(\text{N}_2\text{O}_5)$ is below or equal to the upper limit calculation with equation
743 (3) during both night and day. The largest discrepancy is observed at the beginning of the
744 night, when oxidation of (unsaturated) hydrocarbons by NO_3 (R7) was likely most significant
745 due to the presence of isoprene and other biogenic VOCs. Indeed, if the $\sum k_{\text{NO}_3+\text{VOC},i}[\text{VOC}]_i$ is
746 assumed to be 0.11 s^{-1} (average nocturnal NO_3 loss frequency reported by (Liebmann et al.,
747 2018)), the gap between observed and calculated N_2O_5 lifetime between sunset and midnight
748 closes (Figure S-8). However, this is also the time when the steady state approximation is
749 most likely invalid.

750

751 3.2.3 Heterogeneous conversion of N_2O_5 to ClNO_2 on the night of August 1/2

752 Phillips et al. (2016) recently applied several methods to estimate the N_2O_5 uptake parameter
753 (γ) and yield of ClNO_2 (ϕ) from ambient measurements of NO_3 , N_2O_5 , ClNO_2 , and aerosol
754 nitrate. One of these methods uses the covariance of ClNO_2 and aerosol nitrate production
755 rates, $P(\text{NO}_3^-)$ and $P(\text{ClNO}_2)$:

$$756 \quad \phi = 2(P(\text{NO}_3^-)/P(\text{ClNO}_2) + 1)^{-1} \quad (4)$$

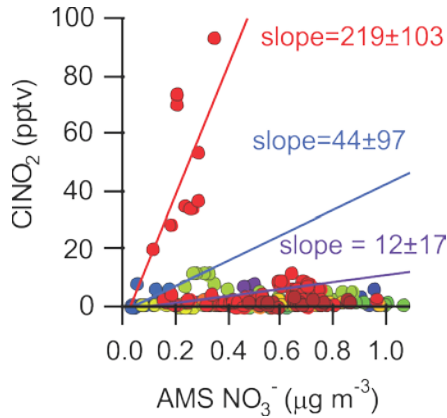
$$757 \quad \gamma = 2(P(\text{NO}_3^-) + P(\text{ClNO}_2)) / (c S_A [\text{N}_2\text{O}_5]) \quad (5)$$

758 In the above equation, c is the mean molecular speed of N_2O_5 ($\approx 237 \text{ m s}^{-1}$). The use of
759 equations (4-5) assumes that the relevant properties of the air mass are conserved (i.e.,
760 identical upwind of and at the measurement location and affected identically by air masses
761 mixing), that losses of measured species are not significant, that the efficiency of N_2O_5 uptake
762 and production of ClNO_2 and NO_3^- is independent of particle size, and the absence of
763 partitioning of $\text{HNO}_{3(\text{g})}$ and aerosol nitrate between the gas and particle phases (Phillips et al.,
764 2016). It is assumed further that production of nitrate from N_2O_5 uptake on refractory aerosol
765 (that the ACSM does not quantify) is minimal.

766 In this data set, ClNO_2 and PM_{10} nitrate rarely covaried (Figure 9); the only instance showing a
767 modest correlation ($r=0.66$) is the time period prior to sunrise of August 2 (shown as red dots
768 in Figure 9).

769

770



771

772 **Figure 9.** Scatter plot of ClNO₂ mixing ratios with submicron (PM₁) ACSM NO₃⁻ data. The
773 slopes were calculated for three periods: Aug 2, 01:25 – 04:55 (red dots; slope = 219±103; ϕ
774 = 0.72), July 23, 03:00 – 04:25 (blue dots slope = 44±97; ϕ = 0.21), and July 21, 02:25 –
775 05:20 (purple dots slope = 12±17; ϕ = 0.06).

776

777 The night of August 1-2 exhibited the highest nocturnal nitrogen oxide concentrations for the
778 entire campaign. Winds were initially from the NW and relatively light (4.8 ± 0.7 km hr⁻¹) and
779 after 01:00 picked up in speed (to 8 ± 1 km hr⁻¹) and shifted to the W. Judging from the HYbrid
780 Single-Particle Lagrangian Integrated Trajectory (HYSPLIT) back trajectories (Draxler and
781 Rolph, 2013), the upwind air had moved in from the coast, roughly from the direction of the
782 city of Victoria, BC (Odame-Ankrah, 2015).

783 After sunset at ~21:00 local time, N₂O₅ levels started increasing and continued to increase
784 until about 01:30 (Figure 3A). The steady state N₂O₅ lifetime at this time was the highest of
785 the campaign, ~10 min. At 01:20, ClNO₂ mixing ratio increased from 20.4 pptv at 01:25 to
786 93.7 pptv at 04:55 and the aerosol nitrate content from 0.10 to 0.34 $\mu\text{g m}^{-3}$ (40 to 127 pptv).
787 During this time, N₂O₅ mixing ratios and PM₁ surface area density were relatively constant,
788 11 ± 6 pptv and 67 ± 4 $\mu\text{g m}^{-3}$ (average \pm standard deviation), respectively. The combined
789 amount of N₂O₅, ClNO₂ and NO₃⁻ produced (172 pptv) is less than the amount of NO₃
790 produced from R1 which was 519 pptv during this period.

791 From equations (4) and (5), a ClNO₂ yield of $\phi = 0.7\pm 0.3$ and an N₂O₅ uptake probability of γ
792 = 0.15 ± 0.07 were calculated for this period. Both of these values are upper limits because

793 production of ClNO₂ from uptake of N₂O₅ on unquantified supermicron (i.e., > 0.5 μm) or
794 refractory aerosol (which takes place simultaneously) is not accounted for.

795 A γ value of > 0.05 is greater than can be rationalized from laboratory and field studies
796 (Chang et al., 2011) and is hence unrealistic. This suggests that ClNO₂ production took place
797 predominantly on supermicron or refractory aerosol, which likely was comprised of mainly
798 sea salt derived aerosol (Anlauf et al., 2006). On the other hand, if one assumes that all of the
799 ClNO₂ is produced on supermicron or refractory aerosol such that P(ClNO₂) on submicron
800 aerosol equals 0 pptv s⁻¹ (which is not unreasonable considering the absence of measurable
801 amounts of aerosol chloride in this size fraction, see section 3.1.5), a γ value of 0.08±0.04 is
802 calculated. This large value suggests very efficient N₂O₅ uptake (and conversion to aerosol
803 nitrate) on the non-refractory submicron aerosol that night.

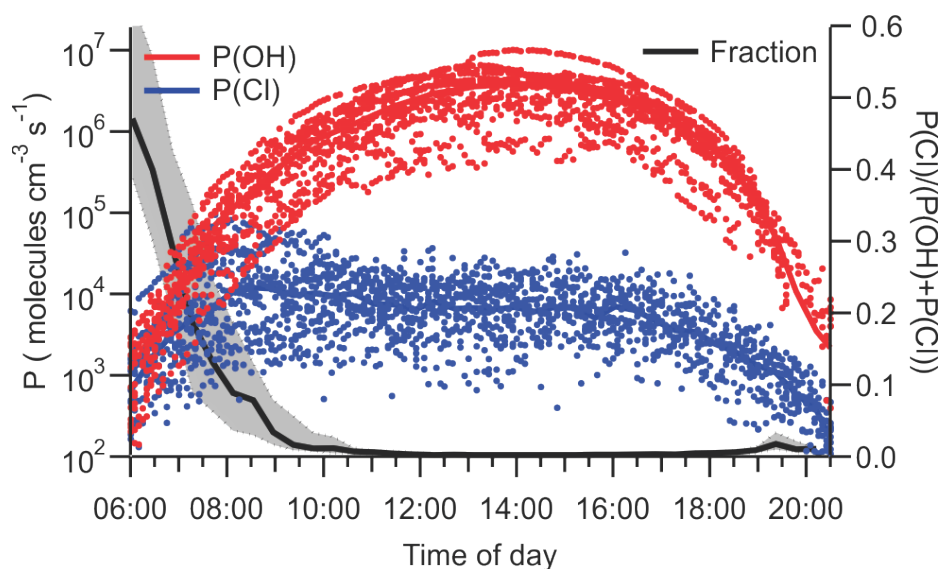
804

805 **3.3 Impacts of ClNO₂ on radical production**

806 Photolysis of ClNO₂ increases the rates of photochemical O₃ production (and hence worsen
807 air quality) by producing NO₂ and reactive Cl atoms (reaction 6). The amounts of ClNO₂
808 available for photolysis in the morning (median 3.5 pptv at sunrise and 6.8 pptv at 08:00 local
809 time) were too small to have had a measurable impact on local NO₂ concentrations (Figure
810 3C) but were sufficiently large to, at least occasionally, impact radical budgets.

811 Figure 10 shows the instantaneous radical production rates of Cl and OH,
812 $P(\text{Cl})=j(\text{ClNO}_2)\times[\text{ClNO}_2]$ and $P(\text{OH})$ from reaction of O(¹D)+H₂O. The latter was calculated
813 from an assumed steady state in O(¹D) with respect to its production from O₃ photolysis and
814 reactions with N₂, O₂, and H₂O as described by Mielke et al. (2016). This analysis does not
815 account for OH radical production from photolysis of nitrous acid or aldehydes and, hence,
816 overestimates the importance of Cl radicals.

817



818

819 **Figure 10.** Plots of instantaneous rates of Cl (blue) and OH (red) radical production from
 820 ClNO₂ photolysis and reaction of O¹D, generated from O₃ photolysis, with H₂O and as a
 821 function of time of day. The fraction of radicals produced from ClNO₂ photolysis is shown in
 822 black. The solid line indicates median values, and shaded areas the 75th and 25th percentiles.

823

824 The largest P(Cl) values were observed on July 26, 07:45 local time (9.5×10^4 atoms $\text{cm}^{-3} \text{s}^{-1}$),
 825 accounting for 40% of the total radical production. The largest fraction of radicals produced
 826 from ClNO₂ photolysis was observed on the same day at 6:35 local time (74%, 7.8×10^3 atoms
 827 $\text{cm}^{-3} \text{s}^{-1}$). The photolysis of ClNO₂ produces a median value of 6.5×10^3 atoms $\text{cm}^{-3} \text{s}^{-1}$ during
 828 daytime, which is negligibly small compared to the median P(OH) of 3.8×10^6 molecules cm^{-3}
 829 s^{-1} at noon.

830

831 **4 Discussion**

832 It is now well-established that ClNO₂ is an abundant nitrogen oxide in many regions of the
833 troposphere (Table 3). The results presented in this paper are atypical in that they show
834 consistently small ClNO₂ mixing ratios in spite of close proximity to sources, i.e., in a region
835 where nearby oceanic emissions of sea salt aerosol and NO_x emissions from a megacity
836 combine. In the following, factors contributing to the low ClNO₂ mixing ratios observed in
837 this study and broader implications of ClNO₂ in the LFV are discussed.

838 The main reason for the low ClNO₂ mixing ratios observed in this work are the low nocturnal
839 mixing ratios of O₃ and small NO₃ production rate, P(NO₃), resulting from the stratification of
840 the boundary layer at night and decoupling of the shallow NBL from the NRL. In the
841 following, it is assumed that a boundary layer structure similar to those observed during
842 PACIFIC 93 (Pisano et al., 1997; McKendry et al., 1997; Hayden et al., 1997) also existed on
843 most measurement nights of this study. Once the nocturnal boundary layer formed at sunset,
844 O₃ and O_x in the NBL were rapidly (lifetime of ~ 4 hours) removed. The box model
845 simulations presented in section 3.2.1 show that this removal can be rationalized by dry
846 deposition and titration of O₃ with NO and biogenic VOCs alone, leaving little room for
847 nitrogen oxide chemistry to destroy O₃ or NO₂, for example, via heterogeneous formation of
848 HONO which destroys NO₂ (Bröske et al., 2003; Stutz et al., 2004a; Indarto, 2012) or
849 formation of N₂O₅ and subsequent heterogeneous hydrolysis which consumes 2 molecules of
850 NO₂ and 1 molecule of O₃ (Brown et al., 2006a). It is the often complete absence of O₃ at
851 night which distinguishes this data set from the other measurement locations for which ClNO₂
852 data have been reported, including continental sites where aerosol chloride is likely less
853 abundant (Table 3).

854 A compounding factor in this study was the occasional formation of fog and occasional
855 precipitation events. Fog droplets act as a very rapid sink for NO₃ and N₂O₅ (Osthoff et al.,
856 2006), which shuts down ClNO₂ production, and may have also directly contributed
857 episodically to ClNO₂ losses, for example on the morning of July 27. Overall, though, the
858 contribution of fog to ClNO₂ losses in this data set was minor, as only 5% of the measurement
859 period was impacted by fog. However, this potential ClNO₂ loss mechanism should be
860 investigated further in future lab studies.

861 The rapid drop of ClNO₂ mixing ratio at around 06:00 of Aug 2 is interesting in that it
862 coincided with a very brief precipitation event. Though an air mass shift cannot be ruled out,

863 this coincidence suggests the possibility that scavenging of ClNO₂ by rain droplets followed
864 by hydrolysis may be a possible loss pathway. Scavenging of NO₃, N₂O₅, and ClNO₂ by rain
865 droplets is currently not constrained by laboratory investigations (unlike other gases, such as
866 SO₂ or NH₃ (Hannemann et al., 1995)). Similarly to fog, precipitation was not a major factor
867 in this data set as it affected only 10% but may be in other locations or seasons that
868 experience higher rainfall amounts.

869 An important observation is the lack of non-refractory PM₁ chloride (Figure 5B). This
870 suggests that there was limited redistribution of chloride from acidification of sea salt aerosol
871 onto other aerosol surfaces in this data set. Such a redistribution was observed, for example,
872 during the Calnex-LA campaign, where the AMS measured a median chloride concentration
873 of ~0.1 μg m⁻³ on non-refractory aerosol (Mielke et al., 2013). This in turn implies that the
874 submicron aerosol surface did not significantly participate in the production of ClNO₂ from
875 N₂O₅ uptake in the NBL, broadly consistent with the conclusions in section 3.2.3 and
876 consistent with measurements of water-soluble aerosol components in the LFV during Pacific
877 2001 (Anlauf et al., 2006) that showed no evidence for chloride redistribution to PM₁ from
878 larger particles where aerosol chloride was present.

879 The low observed τ(N₂O₅) levels are consistent with earlier studies that reported strong
880 vertical gradients in τ(N₂O₅) due to elevated near-surface sinks from emissions by plants (i.e.,
881 monoterpenes) and automobiles (i.e., NO and butadiene (Curren et al., 2006)) that titrate NO₃
882 (Stutz et al., 2004b; Wang et al., 2006; Brown et al., 2007; Young et al., 2012). An
883 emblematic example is the study by Wood et al. (2005) at a ground site east of the San
884 Francisco Bay Area in January 2004: They observed relatively modest N₂O₅ mixing ratios of
885 up to 200 pptv, corresponding to τ(N₂O₅) < 5 min for the entire study period. Studies for
886 which vertically resolved data were available (e.g., (Stutz et al., 2004b; Wang et al., 2006;
887 Brown et al., 2007; Young et al., 2012; Tsai et al., 2014) generally showed higher N₂O₅
888 concentrations and hence larger τ(N₂O₅) aloft in the NRL than at the surface.

889 A different scenario likely played out aloft in the NRL, which would exhibit higher NO₃
890 production rates (via reactions 1) than the surface layer. Assuming levels of 20 ppbv of O₃
891 and NO₂ in the NRL (Pisano et al., 1997; McKendry et al., 1997), the NO₃ production rate
892 would equal ~1.1 ppbv hr⁻¹ in the NRL, roughly on par with values recently reported for Hong
893 Kong, the current record holder for ClNO₂ mixing ratios (Brown et al., 2016; Wang et al.,

894 2016). Recent aircraft and tower studies have shown high rates of production of ClNO₂ aloft
895 (Riedel et al., 2013; Young et al., 2012), which likely also occurred in this work.

896 In contrast, the low mixing height of the NBL is conducive to high levels of biogenic
897 hydrocarbons (section 3.1.6). The nocturnal temperatures during this study were quite warm
898 and did not vary a lot between nights (Figure 8B). Emissions of monoterpenes, which are
899 reactive towards NO₃, are driven by a temperature-dependent process from storage tissue
900 within the plants at night (Guenther et al., 1995) and, hence, were likely substantial. Their
901 presence is likely responsible for the difference between the "observed" N₂O₅ steady
902 lifetimes, $\tau(\text{N}_2\text{O}_5)$, and upper limit calculated using equation (3) before midnight (Figures 8C
903 and S-8). Even if one assumes a relatively large uptake probability of $\gamma=0.025$ and accounts
904 for the large ratios of N₂O₅:NO₃, the loss rate of N₂O₅ on submicron aerosol was likely small
905 in comparison to losses via NO₃ for most of this data set (Figure 7B). Hence, only a small
906 fraction of the integrated nocturnal NO₃ production of 940 pptv resulted in ClNO₂ formation
907 at the surface.

908 Because of the relatively long lifetime of ClNO₂, the breakdown of the surface layer and
909 merging of the surface air with the NRL constituted itself as a ClNO₂ "morning peak" in a
910 similar manner as what has recently been reported at other locations (Tham et al., 2016;
911 Bannan et al., 2015; Faxon et al., 2015). This morning peak is rationalized by higher net
912 ClNO₂ production in the NRL; the break-up of this layer ~2 hours after sunrise then mixes
913 ClNO₂ down to the surface. Such a vertical mixing process was not seen during Calnex-LA
914 (Young et al., 2012; Tsai et al., 2014) where the NBL was sufficiently deep to prevent
915 complete O₃ removal and the ClNO₂ produced mixed down to the surface at night.

916 Assuming a 100 m deep NRL where ClNO₂ production takes place, a mixed layer height of
917 500 m by 08:00 (Pisano et al., 1997) and negligible destruction of ClNO₂ by photolysis
918 (which is reasonable as the lifetime of ClNO₂ with respect to photolysis is >4.6 hours at that
919 time of day), a morning increase in ClNO₂ mixing ratio by 40 pptv at the surface as seen on
920 the morning of July 26 suggests a pool of ClNO₂ in the NRL at sunrise of ~200 pptv, likely a
921 modest value considering that the (assumed) NO₃ production rate may have integrated to ~9
922 ppbv over the course of the night.

923 The largest nocturnal ClNO₂ mixing ratios were observed on July 22/23 and August 1/2. Both
924 of these nights exhibited high wind speeds and are counterexamples to what was observed on
925 other nights. We speculate that the higher levels of wind shear and turbulence altered the

926 nocturnal boundary layer structure which exhibited a greater degree of vertical mixing and
927 higher O₃ concentrations at the surface. Consistent with this interpretation and the notion that
928 an isolated NRL with higher net ClNO₂ production was absent on those nights, the mornings
929 of July 23 and Aug 2 did not show a "morning peak". In contrast, low surface wind speeds
930 were observed on the other nights, facilitating a stable and shallow nocturnal surface layer.

931 It is conceivable that a land-sea breeze effect transported air from a region closer to the coast
932 that saw higher ClNO₂ production than at Abbotsford, i.e., that the ClNO₂ morning peaks are
933 generated by horizontal as opposed to vertical transport. Large NO₃ mixing ratios have been
934 reported at Saturna Island (McLaren et al., 2010), which strongly suggest that sizeable
935 reservoirs of ClNO₂ form offshore at night. However, it is known how far inland these
936 reservoirs extend. Considering the average wind speed in the morning (6 km hr⁻¹), distance to
937 the coast (35 km), and close proximity (200 m) of the site to the bottom of the polluted NRL
938 with documented high nocturnal pollution levels and early morning down mixing events, the
939 vertical transport explanation is much more likely correct. Nevertheless, measurements of
940 ClNO₂ at a site closer to the coast (e.g., at White Rock) would be beneficial.

941 Formation of ClNO₂ affects air quality through its photolysis which generates O_x, NO_x, and
942 reactive Cl radicals in the morning, leading to higher net photochemical O₃ production
943 (Sarwar et al., 2014). In spite of the low levels of ClNO₂ observed in this work, the
944 production of radicals from its photodissociation was not always negligible (Figure 10).
945 Conditions leading to O₃ exceedances did not develop during this study. If such conditions
946 had developed, it is highly likely that this radical generation would have played a much
947 greater role.

948 The data presented here suggest that higher rates of ClNO₂ and subsequent radical generation
949 take place routinely in layers aloft, processes that are not directly observable at the surface but
950 whose implications are felt as the ultimate product, O₃, is sufficiently long-lived to mix down
951 to the surface (McKendry et al., 1997). Future studies should therefore target the NRL, for
952 example through missed-approaches by aircraft, a blimp, or from a tall tower, especially
953 during episodes of a developing O₃ exceedance event and also include composition
954 measurements of refractory aerosol.

955

956 **5 Summary and conclusions**

957 In this paper, we have presented the first measurements of ClNO₂ and N₂O₅ mixing ratios in
958 the LFV. In spite of the close proximity to NO_x (megacity of Vancouver) and sea salt aerosol
959 (the Pacific Ocean) sources, ClNO₂ and N₂O₅ mixing ratios were small (maximum of 97 and
960 27 pptv, respectively) and smaller than observed at other measurement locations for which
961 ClNO₂ abundances were reported. The low mixing ratios are explained through the removal
962 of O₃ by deposition and titration with NO in a shallow nocturnal surface layer. Measurements
963 of submicron aerosol composition by ACSM showed no enhancements of particle-phase
964 chloride, which is in contrast to locations where high ClNO₂ mixing ratios were observed
965 (such as Pasadena (Mielke et al., 2013)) and indicates that there was little processing and
966 redistribution of sea salt derived chloride at this location. There is indirect evidence that
967 higher production of ClNO₂ took place above the measurement site in the NRL, observed via
968 downmixing after the break-up of the NBL in the morning, and highlights the need for future
969 vertically resolved measurements (e.g., from an aircraft platform) of ClNO₂ and N₂O₅ mixing
970 ratios in the LFV. Conditions leading to O₃ exceedences did not develop during the relatively
971 short measurement period of 2 weeks, such that the full impact that nocturnal formation of
972 ClNO₂ could have on radical production and NO₂ recycling remains unquantified.

973

974 **Data availability**

975 The data used in this study are available from the corresponding author upon request
976 (hosthoff@ucalgary.ca).

977

978 **Acknowledgments**

979 This project was undertaken with the financial support of the Government of Canada through
980 the Federal Department of the Environment. Ce projet a été réalisé avec l'appui financier du
981 Gouvernement du Canada agissant par l'entremise du ministère fédéral de l'Environnement.
982 Partial funding for this work was provided by the Natural Sciences and Engineering Research
983 Council of Canada (NSERC) in the form of operating ("Discovery") and Research Tools and
984 Instruments (RTI) grants. The Abbotsford field study was financially supported by a BC Clear
985 research grant from the Fraser Basin Council of British Columbia and by Metro Vancouver.

986

987

988 **References**

- 989 Ainslie, B., and Steyn, D. G.: Spatiotemporal Trends in Episodic Ozone Pollution in the
990 Lower Fraser Valley, British Columbia, in Relation to Mesoscale Atmospheric Circulation
991 Patterns and Emissions, *J. Appl. Met. Climatol.*, 46, 1631-1644, 10.1175/JAM2547.1, 2007.
- 992 Ainslie, B., Steyn, D. G., Reuten, C., and Jackson, P. L.: A Retrospective Analysis of Ozone
993 Formation in the Lower Fraser Valley, British Columbia, Canada. Part II: Influence of
994 Emissions Reductions on Ozone Formation, *Atmosphere-Ocean*, 51, 170-186,
995 10.1080/07055900.2013.782264, 2013.
- 996 Aldener, M., Brown, S. S., Stark, H., Williams, E. J., Lerner, B. M., Kuster, W. C., Goldan, P.
997 D., Quinn, P. K., Bates, T. S., Fehsenfeld, F. C., and Ravishankara, A. R.: Reactivity and loss
998 mechanisms of NO_3 and N_2O_5 in a polluted marine environment: Results from in situ
999 measurements during New England Air Quality Study 2002, *J. Geophys. Res.*, 111, D23S73,
1000 doi:10.1029/2006JD007252, 2006.
- 1001 Alfarra, M. R., Coe, H., Allan, J. D., Bower, K. N., Boudries, H., Canagaratna, M. R.,
1002 Jimenez, J. L., Jayne, J. T., Garforth, A. A., Li, S.-M., and Worsnop, D. R.: Characterization
1003 of urban and rural organic particulate in the Lower Fraser Valley using two Aerodyne Aerosol
1004 Mass Spectrometers, *Atmos. Environm.*, 38, 5745-5758, 10.1016/j.atmosenv.2004.01.054,
1005 2004.
- 1006 Alicke, B., Geyer, A., Hofzumahaus, A., Holland, F., Konrad, S., Patz, H. W., Schafer, J.,
1007 Stutz, J., Volz-Thomas, A., and Platt, U.: OH formation by HONO photolysis during the
1008 BERLIOZ experiment, *J. Geophys. Res.*, 108, 8247, 10.1029/2001JD000579, 2003.
- 1009 Anlauf, K., Li, S.-M., Leaitch, R., Brook, J., Hayden, K., Toom-Sauntry, D., and Wiebe, A.:
1010 Ionic composition and size characteristics of particles in the Lower Fraser Valley: Pacific
1011 2001 field study, *Atmos. Environm.*, 40, 2662-2675, 10.1016/j.atmosenv.2005.12.027, 2006.

1012 Bannan, T. J., Booth, A. M., Bacak, A., Muller, J. B. A., Leather, K. E., Le Breton, M., Jones,
1013 B., Young, D., Coe, H., Allan, J., Visser, S., Slowik, J. G., Furger, M., Prévôt, A. S. H., Lee,
1014 J., Dunmore, R. E., Hopkins, J. R., Hamilton, J. F., Lewis, A. C., Whalley, L. K., Sharp, T.,
1015 Stone, D., Heard, D. E., Fleming, Z. L., Leigh, R., Shallcross, D. E., and Percival, C. J.: The
1016 first UK measurements of nitryl chloride using a chemical ionization mass spectrometer in
1017 central London in the summer of 2012, and an investigation of the role of Cl atom oxidation,
1018 *J. Geophys. Res.*, 120, 5638-5657, 10.1002/2014jd022629, 2015.

1019 Bart, M., Williams, D. E., Ainslie, B., McKendry, I., Salmond, J., Grange, S. K., Alavi-
1020 Shoshtari, M., Steyn, D., and Henshaw, G. S.: High Density Ozone Monitoring Using Gas
1021 Sensitive Semi-Conductor Sensors in the Lower Fraser Valley, British Columbia, *Environm.*
1022 *Sci. Technol.*, 48, 3970-3977, 10.1021/es404610t, 2014.

1023 Behnke, W., George, C., Scheer, V., and Zetzsch, C.: Production and decay of ClNO₂, from
1024 the reaction of gaseous N₂O₅ with NaCl solution: Bulk and aerosol experiments, *J. Geophys.*
1025 *Res.*, 102, 3795-3804, 10.1029/96JD03057 1997.

1026 Bertram, T. H., and Thornton, J. A.: Toward a general parameterization of N₂O₅ reactivity on
1027 aqueous particles: the competing effects of particle liquid water, nitrate and chloride, *Atmos.*
1028 *Chem. Phys.*, 9, 8351-8363, 10.5194/acp-9-8351-2009, 2009.

1029 Biesenthal, T. A., Wu, Q., Shepson, P. B., Wiebe, H. A., Anlauf, K. G., and Mackay, G. I.: A
1030 study of relationships between isoprene, its oxidation products, and ozone, in the Lower
1031 Fraser Valley, BC, *Atmos. Environm.*, 31, 2049-2058, 10.1016/S1352-2310(96)00318-4,
1032 1997.

1033 Boudries, H., Canagaratna, M. R., Jayne, J. T., Alfarra, M. R., Allan, J., Bower, K. N., Coe,
1034 H., Pryor, S. C., Jimenez, J. L., Brook, J. R., Li, S., and Worsnop, D. R.: Chemical and
1035 physical processes controlling the distribution of aerosols in the Lower Fraser Valley, Canada,

1036 during the Pacific 2001 field campaign, *Atmos. Environm.*, 38, 5759-5774,
1037 10.1016/j.atmosenv.2004.01.057, 2004.

1038 Brook, J. R., Strawbridge, K. B., Snyder, B. J., Boudries, H., Worsnop, D., Sharma, S.,
1039 Anlauf, K., Lu, G., and Hayden, K.: Towards an understanding of the fine particle variations
1040 in the LFV: integration of chemical, physical and meteorological observations, *Atmos.*
1041 *Environm.*, 38, 5775-5788, 10.1016/j.atmosenv.2004.01.056, 2004.

1042 Bröske, R., Kleffmann, J., and Wiesen, P.: Heterogeneous conversion of NO₂ on secondary
1043 organic aerosol surfaces: A possible source of nitrous acid (HONO) in the atmosphere?,
1044 *Atmos. Chem. Phys.*, 3, 469-474, 10.5194/acp-3-469-2003, 2003.

1045 Brown, S. S., Stark, H., Ciciora, S. J., and Ravishankara, A. R.: In-situ measurement of
1046 atmospheric NO₃ and N₂O₅ via cavity ring-down spectroscopy, *Geophys. Res. Lett.*, 28, 3227-
1047 3230, 10.1029/2001GL013303, 2001.

1048 Brown, S. S., Stark, H., Ciciora, S. J., McLaughlin, R. J., and Ravishankara, A. R.:
1049 Simultaneous in situ detection of atmospheric NO₃ and N₂O₅ via cavity ring-down
1050 spectroscopy, *Rev. Sci. Instrum.*, 73, 3291-3301, 10.1063/1.1499214, 2002.

1051 Brown, S. S., Stark, H., and Ravishankara, A. R.: Applicability of the steady state
1052 approximation to the interpretation of atmospheric observations of NO₃ and N₂O₅, *J.*
1053 *Geophys. Res.*, 108, 4539, 10.1029/2003JD003407, 2003.

1054 Brown, S. S., Neuman, J. A., Ryerson, T. B., Trainer, M., Dube, W. P., Holloway, J. S.,
1055 Warneke, C., de Gouw, J. A., Donnelly, S. G., Atlas, E., Matthew, B., Middlebrook, A. M.,
1056 Peltier, R., Weber, R. J., Stohl, A., Meagher, J. F., Fehsenfeld, F. C., and Ravishankara, A. R.:
1057 Nocturnal odd-oxygen budget and its implications for ozone loss in the lower troposphere,
1058 *Geophys. Res. Lett.*, 33, L08801, 10.1029/2006GL025900, 2006a.

1059 Brown, S. S., Ryerson, T. B., Wollny, A. G., Brock, C. A., Peltier, R., Sullivan, A. P., Weber,
1060 R. J., Dube, W. P., Trainer, M., Meagher, J. F., Fehsenfeld, F. C., and Ravishankara, A. R.:
1061 Variability in nocturnal nitrogen oxide processing and its role in regional air quality, *Science*,
1062 311, 67-70, 10.1126/science.1120120 2006b.

1063 Brown, S. S., Dube, W. P., Osthoff, H. D., Stutz, J., Ryerson, T. B., Wollny, A. G., Brock, C.
1064 A., Warneke, C., De Gouw, J. A., Atlas, E., Neuman, J. A., Holloway, J. S., Lerner, B. M.,
1065 Williams, E. J., Kuster, W. C., Goldan, P. D., Angevine, W. M., Trainer, M., Fehsenfeld, F.
1066 C., and Ravishankara, A. R.: Vertical profiles in NO₃ and N₂O₅ measured from an aircraft:
1067 Results from the NOAA P-3 and surface platforms during the New England Air Quality Study
1068 2004, *J. Geophys. Res.*, 112, D22304, 10.1029/2007JD008883, 2007.

1069 Brown, S. S., and Stutz, J.: Nighttime radical observations and chemistry, *Chem. Soc. Rev.*,
1070 41, 6405-6447, 10.1039/c2cs35181a, 2012.

1071 Brown, S. S., Thornton, J. A., Keene, W. C., Pszenny, A. A. P., Sive, B. C., Dubé, W. P.,
1072 Wagner, N. L., Young, C. J., Riedel, T. P., Roberts, J. M., VandenBoer, T. C., Bahreini, R.,
1073 Öztürk, F., Middlebrook, A. M., Kim, S., Hübler, G., and Wolfe, D. E.: Nitrogen, Aerosol
1074 Composition, and Halogens on a Tall Tower (NACHTT): Overview of a wintertime air
1075 chemistry field study in the front range urban corridor of Colorado, *J. Geophys. Res.*, 118,
1076 8067-8085, 10.1002/jgrd.50537, 2013.

1077 Brown, S. S., Dubé, W. P., Tham, Y. J., Zha, Q., Xue, L., Poon, S., Wang, Z., Blake, D. R.,
1078 Tsui, W., Parrish, D. D., and Wang, T.: Nighttime chemistry at a high altitude site above
1079 Hong Kong, *J. Geophys. Res.-Atmos.*, 121, 2457-2475, 10.1002/2015jd024566, 2016.

1080 Chang, W. L., Bhave, P. V., Brown, S. S., Riemer, N., Stutz, J., and Dabdub, D.:
1081 Heterogeneous Atmospheric Chemistry, Ambient Measurements, and Model Calculations of

1082 N₂O₅: A Review, *Aerosol Sci. Technol.*, 45, 655 - 685, 10.1080/02786826.2010.551672,
1083 2011.

1084 Crowley, J. N., Schuster, G., Pouvesle, N., Parchatka, U., Fischer, H., Bonn, B., Bingemer,
1085 H., and Lelieveld, J.: Nocturnal nitrogen oxides at a rural mountain-site in south-western
1086 Germany, *Atmos. Chem. Phys.*, 10, 2795-2812, 10.5194/acp-10-2795-2010, 2010.

1087 Curren, K. C., Dann, T. F., and Wang, D. K.: Ambient air 1,3-butadiene concentrations in
1088 Canada (1995–2003): seasonal, day of week variations, trends, and source influences, *Atmos.*
1089 *Environm.*, 40, 170-181, 10.1016/j.atmosenv.2005.09.025, 2006.

1090 Davidovits, P., Kolb, C. E., Williams, L. R., Jayne, J. T., and Worsnop, D. R.: Mass
1091 accommodation and chemical reactions at gas-liquid interfaces, *Chem. Rev.*, 106, 1323-1354,
1092 2006.

1093 HYSPLIT (HYbrid Single-Particle Lagrangian Integrated Trajectory) Model access via
1094 NOAA ARL READY Website <http://ready.arl.noaa.gov/HYSPLIT.php>, 2013.

1095 Drewitt, G. B., Curren, K., Steyn, D. G., Gillespie, T. J., and Niki, H.: Measurement of
1096 biogenic hydrocarbon emissions from vegetation in the Lower Fraser Valley, British
1097 Columbia, *Atmos. Environm.*, 32, 3457-3466, 10.1016/S1352-2310(98)00043-0, 1998.

1098 Dubé, W. P., Brown, S. S., Osthoff, H. D., Nunley, M. R., Ciciora, S. J., Paris, M. W.,
1099 McLaughlin, R. J., and Ravishankara, A. R.: Aircraft instrument for simultaneous, in situ
1100 measurement of NO₃ and N₂O₅ via pulsed cavity ring-down spectroscopy, *Rev. Sci. Instrum.*,
1101 77, 034101, 10.1063/1.2176058, 2006.

1102 Edwards, P. M., Brown, S. S., Roberts, J. M., Ahmadov, R., Banta, R. M., deGouw, J. A.,
1103 Dube, W. P., Field, R. A., Flynn, J. H., Gilman, J. B., Graus, M., Helmig, D., Koss, A.,
1104 Langford, A. O., Lefer, B. L., Lerner, B. M., Li, R., Li, S.-M., McKeen, S. A., Murphy, S. M.,

1105 Parrish, D. D., Senff, C. J., Soltis, J., Stutz, J., Sweeney, C., Thompson, C. R., Trainer, M. K.,
1106 Tsai, C., Veres, P. R., Washenfelder, R. A., Warneke, C., Wild, R. J., Young, C. J., Yuan, B.,
1107 and Zamora, R.: High winter ozone pollution from carbonyl photolysis in an oil and gas basin,
1108 *Nature*, 514, 351-354, 10.1038/nature13767, 2014.

1109 Faxon, C., Bean, J., and Ruiz, L.: Inland Concentrations of Cl₂ and ClNO₂ in Southeast Texas
1110 Suggest Chlorine Chemistry Significantly Contributes to Atmospheric Reactivity,
1111 *Atmosphere*, 6, 1487, 10.3390/atmos6101487, 2015.

1112 Finlayson-Pitts, B. J., Ezell, M. J., and Pitts, J. N.: Formation Of Chemically Active Chlorine
1113 Compounds By Reactions Of Atmospheric NaCl Particles With Gaseous N₂O₅ And ClONO₂,
1114 *Nature*, 337, 241-244, 10.1038/337241a0 1989.

1115 Geyer, A., and Stutz, J.: Vertical profiles of NO₃, N₂O₅, O₃, and NO_x in the nocturnal
1116 boundary layer: 2. Model studies on the altitude dependence of composition and chemistry, *J.*
1117 *Geophys. Res.*, 109, D12307, doi:12310.11029/12003JD004211, 2004.

1118 Ghosh, B., Papanastasiou, D. K., Talukdar, R. K., Roberts, J. M., and Burkholder, J. B.: Nitryl
1119 Chloride (ClNO₂): UV/Vis Absorption Spectrum between 210 and 296 K and O(³P) Quantum
1120 Yield at 193 and 248 nm, *J. Phys. Chem. A*, 116, 5796-5805, 10.1021/jp207389y, 2012.

1121 Guenther, A., Hewitt, C. N., Erickson, D., Fall, R., Geron, C., Graedel, T., Harley, P.,
1122 Klinger, L., Lerdau, M., McKay, W. A., Pierce, T., Scholes, B., Steinbrecher, R., Tallamraju,
1123 R., Taylor, J., and Zimmerman, P.: A Global-Model Of Natural Volatile Organic-Compound
1124 Emissions, *J. Geophys. Res.*, 100, 8873-8892, 10.1029/94JD02950, 1995.

1125 Guenther, A. B., Jiang, X., Heald, C. L., Sakulyanontvittaya, T., Duhl, T., Emmons, L. K.,
1126 and Wang, X.: The Model of Emissions of Gases and Aerosols from Nature version 2.1
1127 (MEGAN2.1): an extended and updated framework for modeling biogenic emissions, *Geosci.*
1128 *Model Dev.*, 5, 1471-1492, 10.5194/gmd-5-1471-2012, 2012.

1129 Gurren, K., Gillespie, T., Steyn, D., Dann, T., and Wang, D.: Biogenic isoprene in the Lower
1130 Fraser Valley, British Columbia, *J. Geophys. Res.-Atmos.*, 103, 25467-25477,
1131 10.1029/98jd01214, 1998.

1132 Hannemann, A. U., Mitra, S. K., and Pruppacher, H. R.: On the scavenging of gaseous
1133 nitrogen compounds by large and small rain drops 1. A wind tunnel and theoretical study of
1134 the uptake and desorption of NH₃ in the presence of CO₂, *J. Atmos. Chem.*, 21, 293-307,
1135 10.1007/bf00696760, 1995.

1136 Hayden, K. L., Anlauf, K. G., Hoff, R. M., Strapp, J. W., Bottenheim, J. W., Wiebe, H. A.,
1137 Froude, F. A., Martin, J. B., Steyn, D. G., and McKendry, I. G.: The vertical chemical and
1138 meteorological structure of the boundary layer in the Lower Fraser Valley during Pacific '93,
1139 *Atmos. Environm.*, 31, 2089-2105, 10.1016/S1352-2310(96)00300-7, 1997.

1140 Hayden, K. L., Anlauf, K. G., Li, S. M., Macdonald, A. M., Bottenheim, J. W., Brook, J. R.,
1141 and Wiebe, H. A.: Characterization of gaseous nitrogen oxides in the Lower Fraser Valley
1142 during Pacific 2001, *Atmos. Environm.*, 38, 5811-5823, 10.1016/j.atmosenv.2003.12.048,
1143 2004.

1144 Heintz, F., Platt, U., Flentje, H., and Dubois, R.: Long-term observation of nitrate radicals at
1145 the Tor station, Kap Arkona (Rugen), *J. Geophys. Res.*, 101, 22891-22910,
1146 10.1029/96JD01549, 1996.

1147 Hewitt, C. N., Ashworth, K., Boynard, A., Guenther, A., Langford, B., MacKenzie, A. R.,
1148 Misztal, P. K., Nemitz, E., Owen, S. M., Possell, M., Pugh, T. A. M., Ryan, A. C., and Wild,
1149 O.: Ground-level ozone influenced by circadian control of isoprene emissions, *Nat. Geosci.*,
1150 4, 671-674, 10.1038/ngeo1271, 2011.

1151 Hofzumahaus, A., Kraus, A., and Muller, M.: Solar actinic flux spectroradiometry: a
1152 technique for measuring photolysis frequencies in the atmosphere, *Appl. Optics*, 38, 4443-
1153 4460, 10.1364/AO.38.004443, 1999.

1154 Indarto, A.: Heterogeneous reactions of HONO formation from NO₂ and HNO₃: a review,
1155 *Res. Chem. Intermed.*, 38, 1029-1041, 10.1007/s11164-011-0439-z, 2012.

1156 Jimenez, J. L., Canagaratna, M. R., Donahue, N. M., Prevot, A. S. H., Zhang, Q., Kroll, J. H.,
1157 DeCarlo, P. F., Allan, J. D., Coe, H., Ng, N. L., Aiken, A. C., Docherty, K. S., Ulbrich, I. M.,
1158 Grieshop, A. P., Robinson, A. L., Duplissy, J., Smith, J. D., Wilson, K. R., Lanz, V. A.,
1159 Hueglin, C., Sun, Y. L., Tian, J., Laaksonen, A., Raatikainen, T., Rautiainen, J., Vaattovaara,
1160 P., Ehn, M., Kulmala, M., Tomlinson, J. M., Collins, D. R., Cubison, M. J., E., Dunlea, J.,
1161 Huffman, J. A., Onasch, T. B., Alfarra, M. R., Williams, P. I., Bower, K., Kondo, Y.,
1162 Schneider, J., Drewnick, F., Borrmann, S., Weimer, S., Demerjian, K., Salcedo, D., Cottrell,
1163 L., Griffin, R., Takami, A., Miyoshi, T., Hatakeyama, S., Shimono, A., Sun, J. Y., Zhang, Y.
1164 M., Dzepina, K., Kimmel, J. R., Sueper, D., Jayne, J. T., Herndon, S. C., Trimborn, A. M.,
1165 Williams, L. R., Wood, E. C., Middlebrook, A. M., Kolb, C. E., Baltensperger, U., and
1166 Worsnop, D. R.: Evolution of Organic Aerosols in the Atmosphere, *Science*, 326, 1525-1529,
1167 10.1126/science.1180353, 2009.

1168 Kercher, J. P., Riedel, T. P., and Thornton, J. A.: Chlorine activation by N₂O₅: simultaneous,
1169 in situ detection of ClNO₂ and N₂O₅ by chemical ionization mass spectrometry, *Atmospheric*
1170 *Measurement Techniques*, 2, 193-204, 10.5194/amt-2-193-2009, 2009.

1171 Kim, M. J., Farmer, D. K., and Bertram, T. H.: A controlling role for the air-sea interface in
1172 the chemical processing of reactive nitrogen in the coastal marine boundary layer, *Proc. Natl.*
1173 *Acad. Sci. U.S.A.*, 111, 3943-3948, 10.1073/pnas.1318694111, 2014.

1174 Kleinman, L., Lee, Y.-N., Springston, S. R., Nunnermacker, L., Zhou, X., Brown, R.,
1175 Hallock, K., Klotz, P., Leahy, D., Lee, J. H., and Newman, L.: Ozone formation at a rural site
1176 in the southeastern United States, *J. Geophys. Res.-Atmos.*, 99, 3469-3482,
1177 10.1029/93jd02991, 1994.

1178 Knipping, E. M., and Dabdub, D.: Impact of chlorine emissions from sea-salt aerosol on
1179 coastal urban ozone, *Environm. Sci. Technol.*, 37, 275-284, 10.1021/es025793z 2003.

1180 Koehler, G., and Wassenaar, L. I.: The stable isotopic composition ($^{37}\text{Cl}/^{35}\text{Cl}$) of dissolved
1181 chloride in rainwater, *Applied Geochemistry*, 25, 91-96, 10.1016/j.apgeochem.2009.10.004,
1182 2010.

1183 Liebmann, J., Karu, E., Sobanski, N., Schuladen, J., Ehn, M., Schallhart, S., Quéléver, L.,
1184 Hellen, H., Hakola, H., Hoffmann, T., Williams, J., Fischer, H., Lelieveld, J., and Crowley, J.
1185 N.: Direct measurement of NO_3 radical reactivity in a boreal forest, *Atmos. Chem. Phys.*, 18,
1186 3799-3815, 10.5194/acp-18-3799-2018, 2018.

1187 Lin, C. H., Lai, C. H., Wu, Y. L., and Chen, M. J.: Simple model for estimating dry
1188 deposition velocity of ozone and its destruction in a polluted nocturnal boundary layer,
1189 *Atmos. Environm.*, 44, 4364-4371, 10.1016/j.atmosenv.2010.07.053, 2010.

1190 Logan, J. A.: Ozone in rural areas of the United States, *J. Geophys. Res.-Atmos.*, 94, 8511-
1191 8532, 10.1029/JD094iD06p08511, 1989.

1192 Madronich, S., and Flocke, S.: Theoretical Estimation of Biologically Effective UV Radiation
1193 at the Earth's Surface, in: *Solar Ultraviolet Radiation*, edited by: Zerefos, C., and Bais, A.,
1194 NATO ASI Series, Springer Berlin Heidelberg, 23-48, 1997.

1195 McKendry, I. G., Steyn, D. G., Lundgren, J., Hoff, R. M., Strapp, W., Anlauf, K., Froude, F.,
1196 Martin, J. B., Banta, R. M., and Olivier, L. D.: Elevated ozone layers and vertical down-

1197 mixing over the Lower Fraser Valley, BC, *Atmos. Environm.*, 31, 2135-2146,
1198 10.1016/S1352-2310(96)00127-6, 1997.

1199 McLaren, R., Salmon, R. A., Liggio, J., Hayden, K. L., Anlauf, K. G., and Leitch, W. R.:
1200 Nighttime chemistry at a rural site in the Lower Fraser Valley, *Atmos. Environm.*, 38, 5837-
1201 5848, 10.1016/j.atmosenv.2004.03.074, 2004.

1202 McLaren, R., Wojtal, P., Majonis, D., McCourt, J., Halla, J. D., and Brook, J.: NO₃ radical
1203 measurements in a polluted marine environment: links to ozone formation, *Atmos. Chem.*
1204 *Phys.*, 10, 4187-4206, 10.5194/acp-10-4187-2010, 2010.

1205 Mielke, L. H., Furgeson, A., and Osthoff, H. D.: Observation of ClNO₂ in a mid-continental
1206 urban environment, *Environm. Sci. Technol.*, 45, 8889-8896, 10.1021/es201955u, 2011.

1207 Mielke, L. H., and Osthoff, H. D.: On quantitative measurements of peroxy-carboxylic nitric
1208 anhydride mixing ratios by thermal dissociation chemical ionization mass spectrometry, *Int. J.*
1209 *Mass Spectrom.*, 310, 1-9, 10.1016/j.ijms.2011.10.005, 2012.

1210 Mielke, L. H., Stutz, J., Tsai, C., Hurlock, S. C., Roberts, J. M., Veres, P. R., Froyd, K. D.,
1211 Hayes, P. L., Cubison, M. J., Jimenez, J. L., Washenfelder, R. A., Young, C. J., Gilman, J. B.,
1212 de Gouw, J. A., Flynn, J. H., Grossberg, N., Lefer, B. L., Liu, J., Weber, R. J., and Osthoff, H.
1213 D.: Heterogeneous formation of nitryl chloride and its role as a nocturnal NO_x reservoir
1214 species during CalNex-LA 2010, *J. Geophys. Res.*, 118, 10638-10652, 10.1002/jgrd.50783,
1215 2013.

1216 Mielke, L. H., Furgeson, A., Odame-Ankrah, C. A., and Osthoff, H. D.: Ubiquity of ClNO₂ in
1217 the nocturnal boundary layer of Calgary, AB, Canada, *Canadian Journal of Chemistry*, 94,
1218 414-423, 10.1139/cjc-2015-0426, 2016.

1219 Neu, U., Kunzle, T., and Wanner, H.: On the relation between ozone storage in the residual
1220 layer and daily variation in near-surface ozone concentration — A case study, *Bound.-Layer*
1221 *Meteor.*, 69, 221-247, 10.1007/bf00708857, 1994.

1222 Ng, N. L., Herndon, S. C., Trimborn, A., Canagaratna, M. R., Croteau, P. L., Onasch, T. B.,
1223 Sueper, D., Worsnop, D. R., Zhang, Q., Sun, Y. L., and Jayne, J. T.: An Aerosol Chemical
1224 Speciation Monitor (ACSM) for Routine Monitoring of the Composition and Mass
1225 Concentrations of Ambient Aerosol, *Aerosol Sci. Technol.*, 45, 780-794,
1226 10.1080/02786826.2011.560211, 2011.

1227 Odame-Ankrah, C. A., and Osthoff, H. D.: A compact diode laser cavity ring-down
1228 spectrometer for atmospheric measurements of NO₃ and N₂O₅ with automated zeroing and
1229 calibration, *Appl. Spectrosc.*, 65, 1260-1268, 10.1366/11-06384, 2011.

1230 Odame-Ankrah, C. A.: Improved detection instrument for nitrogen oxide species, Ph.D.,
1231 Chemistry, University of Calgary, <http://hdl.handle.net/11023/2006>, Calgary, 2015.

1232 Osthoff, H. D., Sommariva, R., Baynard, T., Pettersson, A., Williams, E. J., Lerner, B. M.,
1233 Roberts, J. M., Stark, H., Goldan, P. D., Kuster, W. C., Bates, T. S., Coffman, D.,
1234 Ravishankara, A. R., and Brown, S. S.: Observation of daytime N₂O₅ in the marine boundary
1235 layer during New England Air Quality Study - Intercontinental Transport and Chemical
1236 Transformation 2004, *J. Geophys. Res.*, 111, D23S14, doi:10.1029/2006JD007593., 2006.

1237 Osthoff, H. D., Pilling, M. J., Ravishankara, A. R., and Brown, S. S.: Temperature
1238 dependence of the NO₃ absorption cross-section above 298 K and determination of the
1239 equilibrium constant for NO₃+NO₂ <-> N₂O₅ at atmospherically relevant conditions, *Phys.*
1240 *Chem. Chem. Phys.*, 9, 5785-5793, 10.1039/b709193a, 2007.

1241 Osthoff, H. D., Roberts, J. M., Ravishankara, A. R., Williams, E. J., Lerner, B. M.,
1242 Sommariva, R., Bates, T. S., Coffman, D., Quinn, P. K., Stark, H., Burkholder, J. B.,

1243 Talukdar, R. K., Meagher, J., Fehsenfeld, F. C., and Brown, S. S.: High levels of nitryl
1244 chloride in the polluted subtropical marine boundary layer, *Nat. Geosci.*, 1, 324-328,
1245 10.1038/ngeo177, 2008.

1246 Paul, D., Furgeson, A., and Osthoff, H. D.: Measurement of total alkyl and peroxy nitrates by
1247 thermal decomposition cavity ring-down spectroscopy, *Rev. Sci. Instrum.*, 80, 114101,
1248 10.1063/1.3258204 2009.

1249 Paul, D., and Osthoff, H. D.: Absolute Measurements of Total Peroxy Nitrate Mixing Ratios
1250 by Thermal Dissociation Blue Diode Laser Cavity Ring-Down Spectroscopy, *Anal. Chem.*,
1251 82, 6695-6703, 10.1021/ac101441z, 2010.

1252 Phillips, G. J., Tang, M. J., Thieser, J., Brickwedde, B., Schuster, G., Bohn, B., Lelieveld, J.,
1253 and Crowley, J. N.: Significant concentrations of nitryl chloride observed in rural continental
1254 Europe associated with the influence of sea salt chloride and anthropogenic emissions,
1255 *Geophys. Res. Lett.*, 39, L10811, 10.1029/2012gl051912, 2012.

1256 Phillips, G. J., Thieser, J., Tang, M. J., Sobanski, N., Schuster, G., Fachinger, J., Drewnick,
1257 F., Borrmann, S., Bingemer, H., Lelieveld, J., and Crowley, J. N.: Estimating N₂O₅ uptake
1258 coefficients using ambient measurements of NO₃, N₂O₅, ClNO₂ and particle-phase nitrate,
1259 *Atmos. Chem. Phys.*, 16, 13231-13249, 10.5194/acp-16-13231-2016, 2016.

1260 Pisano, J. T., McKendry, I., Steyn, D. G., and Hastie, D. R.: Vertical nitrogen dioxide and
1261 ozone concentrations measured from a tethered balloon in the Lower Fraser Valley, *Atmos.*
1262 *Environm.*, 31, 2071-2078, 10.1016/S1352-2310(96)00146-X, 1997.

1263 Pryor, S. C., Barthelmie, R. J., Hoff, R. M., Sakiyama, S., Simpson, R., and Steyn, D.:
1264 REVEAL: Characterizing fine aerosols in the Fraser Valley, BC, *Atmosphere-Ocean*, 35,
1265 209-227, 10.1080/07055900.1997.9649592, 1997.

1266 Pryor, S. C., and Barthelmie, R. J.: REVEAL II: Seasonality and spatial variability of particle
1267 and visibility conditions in the Fraser Valley, *Sci. Tot. Environm.*, 257, 95-110,
1268 10.1016/S0048-9697(00)00490-3, 2000.

1269 Pryor, S. C., Barthelmie, R. J., Schoof, J. T., Binkowski, F. S., Delle Monache, L., and Stull,
1270 R.: Modeling the impact of sea-spray on particle concentrations in a coastal city, *Sci. Tot.*
1271 *Environm.*, 391, 132-142, 10.1016/j.scitotenv.2007.10.059, 2008.

1272 Raff, J. D., Njegic, B., Chang, W. L., Gordon, M. S., Dabdub, D., Gerber, R. B., and
1273 Finlayson-Pitts, B. J.: Chlorine activation indoors and outdoors via surface-mediated reactions
1274 of nitrogen oxides with hydrogen chloride, *Proc. Natl. Acad. Sci. U.S.A.*, 106, 13647-13654,
1275 10.1073/pnas.0904195106, 2009.

1276 Riedel, T. P., Bertram, T. H., Crisp, T. A., Williams, E. J., Lerner, B. M., Vlasenko, A., Li,
1277 S.-M., Gilman, J. B., de Gouw, J., Bon, D. M., Wagner, N. L., Brown, S. S., and Thornton, J.
1278 A.: Nitryl Chloride and Molecular Chlorine in the Coastal Marine Boundary Layer,
1279 *Environm. Sci. Technol.*, 46, 10463-10470, 10.1021/es204632r, 2012a.

1280 Riedel, T. P., Bertram, T. H., Ryder, O. S., Liu, S., Day, D. A., Russell, L. M., Gaston, C. J.,
1281 Prather, K. A., and Thornton, J. A.: Direct N_2O_5 reactivity measurements at a polluted coastal
1282 site, *Atmos. Chem. Phys.*, 12, 2959-2968, 10.5194/acp-12-2959-2012, 2012b.

1283 Riedel, T. P., Wagner, N. L., Dubé, W. P., Middlebrook, A. M., Young, C. J., Öztürk, F.,
1284 Bahreini, R., VandenBoer, T. C., Wolfe, D. E., Williams, E. J., Roberts, J. M., Brown, S. S.,
1285 and Thornton, J. A.: Chlorine activation within urban or power plant plumes: Vertically
1286 resolved $ClNO_2$ and Cl_2 measurements from a tall tower in a polluted continental setting, *J.*
1287 *Geophys. Res.*, 118, 8702-8715, 10.1002/jgrd.50637, 2013.

1288 Roberts, J. M., Osthoff, H. D., Brown, S. S., Ravishankara, A. R., Coffman, D., Quinn, P. K.,
1289 and Bates, T. S.: Laboratory Studies of Products of N₂O₅ Uptake on Cl⁻ Containing
1290 Substrates, *Geophys. Res. Lett.*, 36, L20808, 10.1029/2009GL040448, 2009.

1291 Ryder, O. S., Ault, A. P., Cahill, J. F., Guasco, T. L., Riedel, T. P., Cuadra-Rodriguez, L. A.,
1292 Gaston, C. J., Fitzgerald, E., Lee, C., Prather, K. A., and Bertram, T. H.: On the Role of
1293 Particle Inorganic Mixing State in the Reactive Uptake of N₂O₅ to Ambient Aerosol Particles,
1294 *Environm. Sci. Technol.*, 48, 1618-1627, 10.1021/es4042622, 2014.

1295 Ryder, O. S., Campbell, N. R., Morris, H., Forestieri, S., Ruppel, M. J., Cappa, C., Tivanski,
1296 A., Prather, K., and Bertram, T. H.: Role of Organic Coatings in Regulating N₂O₅ Reactive
1297 Uptake to Sea Spray Aerosol, *J. Phys. Chem. A*, 119, 11683-11692,
1298 10.1021/acs.jpca.5b08892, 2015a.

1299 Ryder, O. S., Campbell, N. R., Shaloski, M., Al-Mashat, H., Nathanson, G. M., and Bertram,
1300 T. H.: Role of Organics in Regulating ClNO₂ Production at the Air–Sea Interface, *J. Phys.*
1301 *Chem. A*, 119, 8519-8526, 10.1021/jp5129673, 2015b.

1302 Sander, R., and Crutzen, P. J.: Model study indicating halogen activation and ozone
1303 destruction in polluted air masses transported to the sea, *J. Geophys. Res.*, 101, 9121-9138,
1304 10.1029/95JD03793, 1996.

1305 Sander, S. P., Abbatt, J. P. D., Barker, J. R., Burkholder, J. B., Friedl, R. R., Golden, D. M.,
1306 Huie, R. E., Kolb, C. E., Kurylo, M. J., Moortgat, G. K., Orkin, V. L., and Wine, P. H.:
1307 Chemical Kinetics and Photochemical Data for Use in Atmospheric Studies, Evaluation No.
1308 17, JPL Publication 10-6, Jet Propulsion Laboratory, Pasadena, CA, 2010.

1309 Sarwar, G., Simon, H., Xing, J., and Mathur, R.: Importance of tropospheric ClNO₂ chemistry
1310 across the Northern Hemisphere, *Geophys. Res. Lett.*, 41, 4050-4058, 10.1002/2014gl059962,
1311 2014.

1312 Seinfeld, J. H., and Pandis, S. N.: Atmospheric chemistry and physics: from air pollution to
1313 climate change, 2nd ed., Wiley, Hoboken, N.J., 2006.

1314 Simpson, W. R.: Continuous wave cavity ring-down spectroscopy applied to in situ detection
1315 of dinitrogen pentoxide (N₂O₅), *Rev. Sci. Instrum.*, 74, 3442-3452, 10.1063/1.1578705, 2003.

1316 Slusher, D. L., Huey, L. G., Tanner, D. J., Flocke, F. M., and Roberts, J. M.: A thermal
1317 dissociation-chemical ionization mass spectrometry (TD-CIMS) technique for the
1318 simultaneous measurement of peroxyacyl nitrates and dinitrogen pentoxide, *J. Geophys. Res.*,
1319 109, D19315, 10.1029/2004JD004670, 2004.

1320 Steyn, D. G., Bottenheim, J. W., and Thomson, R. B.: Overview of tropospheric ozone in the
1321 Lower Fraser Valley, and the Pacific '93 field study, *Atmos. Environm.*, 31, 2025-2035,
1322 10.1016/S1352-2310(97)00018-6, 1997.

1323 Stutz, J., Alicke, B., Ackermann, R., Geyer, A., Wang, S. H., White, A. B., Williams, E. J.,
1324 Spicer, C. W., and Fast, J. D.: Relative humidity dependence of HONO chemistry in urban
1325 areas, *J. Geophys. Res.*, 109, D03307, 10.1029/2003JD004135, 2004a.

1326 Stutz, J., Alicke, B., Ackermann, R., Geyer, A., White, A., and Williams, E.: Vertical profiles
1327 of NO₃, N₂O₅, O₃, and NO_x in the nocturnal boundary layer: 1. Observations during the Texas
1328 Air Quality Study 2000, *J. Geophys. Res.*, 109, D12306, doi:12310.11029/12003JD004209,
1329 2004b.

1330 Talbot, R., Mao, H. T., and Sive, B.: Diurnal characteristics of surface level O₃ and other
1331 important trace gases in New England, *J. Geophys. Res.*, 110, D09307,
1332 doi:09310.01029/02004JD005449, 2005.

1333 Tanaka, P. L., Riemer, D. D., Chang, S. H., Yarwood, G., McDonald-Buller, E. C., Apel, E.
1334 C., Orlando, J. J., Silva, P. J., Jimenez, J. L., Canagaratna, M. R., Neece, J. D., Mullins, C. B.,

1335 and Allen, D. T.: Direct evidence for chlorine-enhanced urban ozone formation in Houston,
1336 Texas, *Atmos. Environm.*, 37, 1393-1400, 10.1016/S1352-2310(02)01007-5 2003.

1337 Thaler, R. D., Mielke, L. H., and Osthoff, H. D.: Quantification of Nitryl Chloride at Part Per
1338 Trillion Mixing Ratios by Thermal Dissociation Cavity Ring-Down Spectroscopy, *Anal.*
1339 *Chem.*, 83, 2761-2766, 10.1021/ac200055z, 2011.

1340 Tham, Y., Yan, C., Xue, L., Zha, Q., Wang, X., and Wang, T.: Presence of high nitryl
1341 chloride in Asian coastal environment and its impact on atmospheric photochemistry, *Chin.*
1342 *Sci. Bull.*, 59, 356-359, 10.1007/s11434-013-0063-y, 2014.

1343 Tham, Y. J., Wang, Z., Li, Q., Yun, H., Wang, W., Wang, X., Xue, L., Lu, K., Ma, N., Bohn,
1344 B., Li, X., Kecorius, S., Größ, J., Shao, M., Wiedensohler, A., Zhang, Y., and Wang, T.:
1345 Significant concentrations of nitryl chloride sustained in the morning: investigations of the
1346 causes and impacts on ozone production in a polluted region of northern China, *Atmos.*
1347 *Chem. Phys.*, 16, 14959-14977, 10.5194/acp-16-14959-2016, 2016.

1348 Thieser, J., Schuster, G., Schuladen, J., Phillips, G. J., Reiffs, A., Parchatka, U., Pöhler, D.,
1349 Lelieveld, J., and Crowley, J. N.: A two-channel thermal dissociation cavity ring-down
1350 spectrometer for the detection of ambient NO₂, RO₂NO₂ and RONO₂, *Atmos. Meas. Tech.*,
1351 9, 553-576, 10.5194/amt-9-553-2016, 2016.

1352 Thornton, J. A., Kercher, J. P., Riedel, T. P., Wagner, N. L., Cozic, J., Holloway, J. S., Dube,
1353 W. P., Wolfe, G. M., Quinn, P. K., Middlebrook, A. M., Alexander, B., and Brown, S. S.: A
1354 large atomic chlorine source inferred from mid-continental reactive nitrogen chemistry,
1355 *Nature*, 464, 271-274, 10.1038/nature08905, 2010.

1356 Tokarek, T. W., Huo, J. A., Odame-Ankrah, C. A., Hammoud, D., Taha, Y. M., and Osthoff,
1357 H. D.: A gas chromatograph for quantification of peroxy-carboxylic nitric anhydrides

1358 calibrated by thermal dissociation cavity ring-down spectroscopy, *Atmos. Meas. Tech.*, 7,
1359 3263-3283, 10.5194/amt-7-3263-2014, 2014.

1360 Trainer, M., Williams, E. J., Parrish, D. D., Buhr, M. P., Allwine, E. J., Westberg, H. H.,
1361 Fehsenfeld, F. C., and Liu, S. C.: Models and observations of the impact of natural
1362 hydrocarbons on rural ozone, *Nature*, 329, 705-707, 10.1038/329705a0, 1987.

1363 Tsai, C., Wong, C., Hurlock, S., Pikelnaya, O., Mielke, L. H., Osthoff, H. D., Flynn, J. H.,
1364 Haman, C., Lefer, B., Gilman, J., de Gouw, J., and Stutz, J.: Nocturnal loss of NO_x during the
1365 2010 CalNex-LA study in the Los Angeles Basin, *J. Geophys. Res.*, 119, 13004–13025
1366 10.1002/2014jd022171, 2014.

1367 Vingarzan, R., and Li, S. M.: The Pacific 2001 Air Quality Study - synthesis of findings and
1368 policy implications, *Atmos. Environm.*, 40, 2637-2649, 10.1016/j.atmosenv.2005.09.083,
1369 2006.

1370 Volpe, C., Wahlen, M., Pszenny, A. A. P., and Spivack, A. J.: Chlorine isotopic composition
1371 of marine aerosols: Implications for the release of reactive chlorine and HCl cycling rates,
1372 *Geophys. Res. Lett.*, 25, 3831-3834, 10.1029/1998gl900038, 1998.

1373 Wagner, N. L., Dube, W. P., Washenfelder, R. A., Young, C. J., Pollack, I. B., Ryerson, T. B.,
1374 and Brown, S. S.: Diode laser-based cavity ring-down instrument for NO₃, N₂O₅, NO, NO₂
1375 and O₃ from aircraft, *Atmospheric Measurement Techniques*, 4, 1227-1240, 10.5194/amt-4-
1376 1227-2011, 2011.

1377 Wang, S., Ackermann, R., and Stutz, J.: Vertical profiles of O₃ and NO_x chemistry in the
1378 polluted nocturnal boundary layer in Phoenix, AZ: I. Field observations by long-path DOAS,
1379 *Atmos. Chem. Phys.*, 6, 2671-2693, 10.5194/acp-6-2671-2006, 2006.

1380 Wang, T., Tham, Y. J., Xue, L., Li, Q., Zha, Q., Wang, Z., Poon, S. C. N., Dubé, W. P.,
1381 Blake, D. R., Louie, P. K. K., Luk, C. W. Y., Tsui, W., and Brown, S. S.: Observations of
1382 nitryl chloride and modeling its source and effect on ozone in the planetary boundary layer of
1383 southern China, *J. Geophys. Res.-Atmos.*, 121, 2476-2489, 10.1002/2015jd024556, 2016.

1384 Wang, X., Wang, H., Xue, L., Wang, T., Wang, L., Gu, R., Wang, W., Tham, Y. J., Wang, Z.,
1385 Yang, L., Chen, J., and Wang, W.: Observations of N₂O₅ and ClNO₂ at a polluted urban
1386 surface site in North China: High N₂O₅ uptake coefficients and low ClNO₂ product yields,
1387 *Atmos. Environm.*, 156, 125-134, 10.1016/j.atmosenv.2017.02.035, 2017.

1388 Wayne, R. P., Barnes, I., Biggs, P., Burrows, J. P., Canosamas, C. E., Hjorth, J., Lebras, G.,
1389 Moortgat, G. K., Perner, D., Poulet, G., Restelli, G., and Sidebottom, H.: The Nitrate Radical
1390 - Physics, Chemistry, and the Atmosphere, *Atmos. Environm. A*, 25, 1-203, 10.1016/0960-
1391 1686(91)90192-A, 1991.

1392 Wieser, M. E., and Berglund, M.: Atomic weights of the elements 2007 (IUPAC Technical
1393 Report), *Pure Appl. Chem.*, 81, 2131-2156, 10.1351/pac-rep-09-08-03, 2009.

1394 Wild, R. J., Dubé, W. P., Aikin, K. C., Eilerman, S. J., Neuman, J. A., Peischl, J., Ryerson, T.
1395 B., and Brown, S. S.: On-road measurements of vehicle NO₂/NO_x emission ratios in Denver,
1396 Colorado, USA, *Atmos. Environm.*, 148, 182-189, 10.1016/j.atmosenv.2016.10.039, 2017.

1397 Wood, E. C., Bertram, T. H., Wooldridge, P. J., and Cohen, R. C.: Measurements of N₂O₅,
1398 NO₂, and O₃ east of the San Francisco Bay, *Atmos. Chem. Phys.*, 5, 483-491, 10.5194/acp-5-
1399 483-2005, 2005.

1400 Young, C. J., Washenfelder, R. A., Roberts, J. M., Mielke, L. H., Osthoff, H. D., Tsai, C.,
1401 Pikelnaya, O., Stutz, J., Veres, P. R., Cochran, A. K., VandenBoer, T. C., Flynn, J.,
1402 Grossberg, N., Haman, C. L., Lefer, B., Stark, H., Graus, M., de Gouw, J., Gilman, J. B.,
1403 Kuster, W. C., and Brown, S. S.: Vertically Resolved Measurements of Nighttime Radical

1404 Reservoirs in Los Angeles and Their Contribution to the Urban Radical Budget, *Environm.*
1405 *Sci. Technol.*, 46, 10965-10973, 10.1021/es302206a, 2012.

1406 Young, C. J., Washenfelder, R. A., Edwards, P. M., Parrish, D. D., Gilman, J. B., Kuster, W.
1407 C., Mielke, L. H., Osthoff, H. D., Tsai, C., Pikelnaya, O., Stutz, J., Veres, P. R., Roberts, J.
1408 M., Griffith, S., Dusanter, S., Stevens, P. S., Flynn, J., Grossberg, N., Lefer, B., Holloway, J.
1409 S., Peischl, J., Ryerson, T. B., Atlas, E. L., Blake, D. R., and Brown, S. S.: Chlorine as a
1410 primary radical: evaluation of methods to understand its role in initiation of oxidative cycles,
1411 *Atmos. Chem. Phys.*, 14, 3427-3440, 10.5194/acp-14-3427-2014, 2014.

1412 Zhang, Q., Jimenez, J. L., Worsnop, D. R., and Canagaratna, M.: A case study of urban
1413 particle acidity and its influence on secondary organic aerosol, *Environm. Sci. Technol.*, 41,
1414 3213-3219, 10.1021/es061812j, 2007.

1415

1416

1417 **Table 1.** Summary of measurement techniques deployed at T45 during the study.

Species or parameter	Method	Uncertainty	Time resolution
CINO ₂ , PAN, PPN	Chemical ionization mass spectrometry (Mielke et al., 2011)	±25% ±10%	30 s
N ₂ O ₅	Red diode laser cavity ring-down spectroscopy (Odame-Ankrah and Osthoff, 2011)	±25%	1 s
O ₃	UV absorption (Thermo 49i)	±10%	10 s
NO/NO _y	O ₃ -Chemiluminescence (Thermo 42i-Y) with heated Mo converter; operated with inlet filter	±30%	10 s
NO ₂	Blue diode laser cavity ring-down spectroscopy (Paul and Osthoff, 2010)	±10%	1 s
PAN, PPN	Gas chromatography with electron capture detection (Tokarek et al., 2014)	±10%	6 min
Photolysis frequencies	Spectral radiometry (Metcon)	±20%	10 s
Aerosol size distribution	Scanning mobility particle sizer (SMPS)		nd
Aerosol composition	Aerosol Chemical Speciation Monitor (ACSM)	±20%	30 min
VOCs	Agilent	±30%	20 min (1 hr*)
Meteorological data	Various		

1418 * Sampled for 20 min within a 1 hour time period

1419 **Table 2.** Ratios of up- to down-welling photolysis frequencies.

Frequency	Ratio
$j(\text{NO}_3)$	0.27 ± 0.04
$j(\text{NO}_2)$	0.15 ± 0.03
$j(\text{ClNO}_2)$	0.14 ± 0.02
$j(\text{O}_3 \rightarrow \text{O}(^1\text{D}))$	0.11 ± 0.02

1420

1421 **Table 3.** Maximum ClNO₂ mixing ratios observed to date.

Location	Type	Maximum mixing ratio	Reference(s)
Houston, TX	Off-shore, costal, and inland	1.2 ppbv	(Osthoff et al., 2008)
New England	Off-shore	90 pptv	(Kercher et al., 2009)
Pasadena, CA	Off-shore	2.15 ppbv	(Riedel et al., 2012a)
La Jolla, CA	Coastal	30 pptv	(Kim et al., 2014)
Boulder, CO	Continental	425 pptv	(Thornton et al., 2010)
Calgary, AB	Continental	330 pptv	(Mielke et al., 2016; Mielke et al., 2011)
Erie, CO	Continental	1.3 ppbv	(Riedel et al., 2013; Brown et al., 2013)
Feldberg, GER	Continental	800 pptv	(Phillips et al., 2012; Phillips et al., 2016)
Horsepool, UT	Continental	500 pptv	(Edwards et al., 2014)
Pasadena, CA	Coastal, inland	3.5 ppbv	(Mielke et al., 2013)
London, UK	Coastal, inland	724 pptv	(Bannan et al., 2015)
Hongkong, PRC	Coastal, inland	2.0 ppbv	(Tham et al., 2014)
Southeast TX	Coastal, inland	280 pptv	(Faxon et al., 2015)
Hongkong, PRC	Coastal, inland	4.7 ppbv	(Wang et al., 2016)
North China Plain	Continental	2.1 ppbv	(Tham et al., 2016)
North China Plain	Continental	776 pptv	(Wang et al., 2017)
Abbotsford, BC	Coastal, inland	97 pptv	This work

1422